Quantifying atmosphere and ocean origins of North American precipitation variability

Quantifying Atmosphere and Ocean origins of North American Precipitation Variability

Honghai Zhang[1*], Richard Seager[1], Jie He[2], Hansheng Diao[3] and Salvatore Pascale[4]

1. Lamont-Doherty Earth Observatory, Columbia University, Palisades, New York, USA
2. School of Earth and Atmospheric Sciences, Georgia Institute of Technology, Atlanta, Georgia, USA
3. Yau Mathematical Sciences Center, Tsinghua University, Beijing, China
4. Department of Earth System Science, Stanford University, Stanford, California, USA

* Corresponding author: Honghai Zhang (clarkzhang2009@gmail.com; hhzhang@ldeo.columbia.edu), ORCID: 0000-0001-6838-4950

Abstract

How atmospheric and oceanic processes control North American precipitation variability has been extensively investigated, and yet debates remain. Here we address this question in a 50km-resolution flux-adjusted global climate model. The high spatial resolution and flux adjustment greatly improve the model's ability to realistically simulate North American precipitation, the relevant tropical and midlatitude variability and their teleconnections. Comparing two millennium-long simulations with and without an interactive ocean, we find that the leading modes of North American precipitation variability on seasonal and longer timescales exhibit nearly identical spatial and spectral characteristics, explained fraction of total variance and associated atmospheric circulation. This finding suggests that these leading modes arise from internal atmospheric dynamics and atmosphere-land coupling. However, in the fully coupled simulation, North American precipitation variability still correlates significantly with tropical ocean variability, consistent with observations and prior literature. We find that tropical ocean variability does not create its own type of atmospheric variability but excites internal atmospheric modes of variability in midlatitudes. This oceanic impact on North American precipitation is secondary to atmospheric impacts based on correlation. However, relative to the simulation without an interactive ocean, the fully coupled simulation amplifies precipitation variance over southwest North America (SWNA) during late spring to summer by up to 90%. The amplification is caused by a stronger variability in atmospheric moisture content that is attributed to tropical Pacific sea surface temperature variability. Enhanced atmospheric moisture variations over the tropical Pacific are transported by seasonal mean southwesterly winds into SWNA, resulting in larger precipitation variance.

1. Introduction

Precipitation over North America, a region prone to frequent large-scale droughts persisting from a season to multiple decades (e.g., Seager and Ting 2017), has been extensively studied over the past forty years with a goal to assess its predictability and improve predictions. Most of the efforts have been focused on the physical understanding of North American precipitation variability. Processes underlying North American (or any regional) precipitation variability can be categorized into two types, external radiative forcing and internal climate dynamics. In this work we focus on the latter, which consists of processes internal to, and interactions among, atmosphere, land, cryosphere and ocean, on seasonal and longer timescales.

Precipitation is a meteorological phenomenon and the earliest studies are, as expected, atmosphere-oriented. The most prominent large-scale atmosphere circulation variability that have been identified to affect North American precipitation includes the Pacific North America (PNA) pattern (Wallace and Gutzler 1981) and the North Pacific Oscillation (NPO) pattern (Walker 1924). Both patterns represent variations of background mean flow over the North Pacific/America sector. The PNA depicts planetary-scale coherent strengthening or weakening of a trough in the central North Pacific, a ridge over the Rocky Mountains and a trough over southeast North America, while the NPO delineates the meridional movements of the Asian-Pacific jet. The PNA and NPO affect North American precipitation by modulating the Pacific storm track and moisture transport into North America (e.g., Leathers et al. 1991; Linkin and Nigam 2008; Liu et al. 2017; Chen et al. 2018; references therein). Although the PNA and NPO are often portrayed as atmosphere circulation variability, they especially the PNA can also be triggered by ocean variability (e.g., Horel and Wallace 1981) and act as a teleconnection to link remote ocean impacts to North American precipitation variability (Liu et al. 2017).

The tropical ocean's role in North American precipitation variability began to be noticed and understood first by Bjerknes (1966, 1969) and then in the late 1970s and early 1980s, when the now-well-established Rossby wave and teleconnection dynamics were theorized (Hoskins and Karoly 1981) and applied to link the tropical Pacific El Niño-Southern Oscillation (ENSO) to meteorological anomalies over North America (Rasmusson and Wallace 1983). Rossby waves excited by ENSO-induced rainfall anomalies in the tropical Pacific propagate poleward and eastward along a great circle of the Earth and generate alternating cyclonic and anticyclonic circulation anomalies that are quasi-stationary and akin to the PNA pattern, with centers of

action over the North Pacific, western Canada and the southeastern United States. These circulation anomalies affect the strength and position of the subtropical jet stream over the North Pacific (stronger and further equatorward during warm El Niño events and vice versa during cold La Niña events), which then change the associated storminess, moisture transport and precipitation over North America. This dynamical mechanism has been tested in models (e.g., Palmer and Mansfield 1984, 1986; Suarez 1985) and invoked to explain the observed precipitation variations over North America during major ENSO events (e.g., Ropelewski and Halpert 1986; Trenberth et al. 1988; Palmer and Branković 1989; Trenberth and Branstator 1992; Trenberth and Guillemot 1996; Hoerling and Kumar 2003; Schubert et al. 2009). It has also been shown to operate during non-ENSO seasons such as boreal summer, although the associated atmosphere teleconnection pattern changes with seasonal mean circulation (e.g., Castro et al. 2001; and references therein).

The ENSO teleconnection mechanism has been expanded by Seager et al. (2003, 2005). They use observations and models to show that ENSO drives a prominent zonally and hemispherically symmetric component of precipitation variability in the midlatitudes. El Niño events warm the entire tropical troposphere, which strengthens the subtropical jets in both hemispheres and pulls them equatorward (opposite for La Niña events). These changes in the subtropical jets influence the transient eddy momentum fluxes and the eddy-driven mean meridional circulation, resulting in ascent and more precipitation in the midlatitudes especially over North America (Seager et al. 2005a).

On decadal to multidecadal time scales, in the early 2000s, tropical Pacific low-frequency variability was found to affect North American precipitation (e.g., McCabe et al. 2004; Schubert et al. 2004a, b; Seager et al. 2005b). Over the past two decades, tremendous progress has been made, particularly on decadal droughts over North America (see two review papers by Seager and Hoerling 2014; Seager and Ting 2017; and the references therein). The dynamical mechanisms on low-frequency timescales are essentially the same as those on seasonal and interannual timescales as discussed above.

In addition to the tropical Pacific, tropical North Atlantic variability also influences North American precipitation on seasonal to multidecadal timescales (e.g., Enfield et al. 2001; Sutton and Hodson 2005, 2007; Wang et al. 2008; Kushnir et al. 2010; Ruprich-Robert et al. 2016, 2018; Johnson et al. 2020). The associated mechanisms are insensitive to timescales (as for the

tropical Pacific), but seasonally dependent (Kushnir et al. 2010). In warm seasons, variations in tropical North Atlantic sea surface temperature (SST) change the strength of the North Atlantic subtropical high (warmer SSTs lead to a weaker high), which influences the associated northward moisture transport on its west flank from the Gulf of Mexico and thus precipitation over North America (mainly the United States and northern Mexico). In cold seasons, the above warm-season mechanism still operates; in addition, tropical North Atlantic SST variations also modify the convection over the equatorial Pacific, which then affects North American precipitation in a way similar to the ENSO teleconnection but with a weaker amplitude. Overall, the impacts of tropical North Atlantic on North American precipitation are considerably weaker than those from the tropical Pacific.

Despite the significant progress on the physical understanding of North American precipitation variability, debates still remain. For example, the argument that the 1988 summer North American drought was caused by the La Niña event that year (Trenberth et al. 1988; Palmer and Branković 1989) has been refuted by others arguing a fundamental role for remote diabatic heating over the western North Pacific as well as local land feedbacks and atmosphere dynamics (Lyon and Dole 1995; Liu et al. 1998; Chen and Newman 1998; Bates et al. 2001, Seager and Hoerling 2014). The attribution of the infamous 1930s Dust Bowl to the persistent cold tropical Pacific and warm tropical North Atlantic (Schubert et al. 2004a, b; Seager et al. 2005b; Herweijer et al. 2006) has been augmented by studies arguing for an indispensable role for human-induced land changes and dust aerosol feedbacks in the persistence, intensification and spatial expansion of the drought (Cook et al. 2009, 2011) and a fundamental role for atmosphere random processes in the onset of the drought (Hoerling et al. 2009). At the core of these debates is a lack of agreement on the relative contributions to North American precipitation of the tropical oceans and internal atmosphere dynamics—processes internal or intrinsic to the atmosphere and independent of other components of the earth system.

The role of internal atmosphere dynamics in North American precipitation variability on seasonal and longer time scales has been emphasized by a few studies (e.g., Hoerling and Kumar 1997; Hoerling et al. 2009; Seager and Hoerling 2014; Stevenson et al. 2014; Seager and Ting 2017; Kumar and Chen 2020). On seasonal to interannual time scales, North American precipitation anomalies during El Niño events differ significantly from event to event (Rasmusson and Wallace 1983), and most of these differences have been attributed to internal

atmosphere variability (Hoerling and Kumar 1997). On decadal time scales, Stevenson et al. (2017) explore the causes of North American megadroughts by comparing a fully coupled simulation with an atmosphere-only simulation driven by climatological SSTs from the coupled simulation. They find similar intensity and frequency of megadroughts between the two simulations and suggest that the atmosphere alone (still coupled with the land) is able to generate North American megadroughts. A recent review paper by Seager and Ting (2017) conclude that the ocean's role in North American decadal droughts is influential, but not paramount, with atmosphere internal variability explaining up to three quarters of the low-frequency precipitation variability. In all of these studies except Stevenson et al., the role of internal atmosphere dynamics is not explicitly assessed, but inferred as a residual between the total precipitation variations and the ocean contributions that are explicitly assessed (often by averaging ensembles of atmosphere-only simulations driven by observed monthly SSTs). Even in Stevenson et al., internal atmosphere dynamics are only assessed as a whole in terms of the statistics of North American megadroughts. It remains unclear how exactly internal atmosphere dynamics work together with ocean variability to generate North American precipitation variability, especially on seasonal and longer timescales.

In this work, we aim to fill this gap by (1) investigating the specific role of internal atmosphere dynamics in North American precipitation variability on seasonal and longer time scales and (2) assessing how atmospheric and oceanic processes play out in the context of North American precipitation variability, that is, how different or comparable the atmosphere-induced and ocean-induced precipitation variability are. We will not only demonstrate the fundamental role of internal atmospheric dynamics and coupling with land in shaping the spatial and spectral characteristics of the leading modes of variability in North American precipitation, but also present a new physical mechanism whereby the tropical oceans affect North American precipitation variability.

2. Methods

2.1 Model and experiments

In order to cleanly separate the contributions of atmospheric and oceanic processes, analyzing observations alone is not enough and we have to use climate models. The model in this work is the Forecast-oriented Low Ocean Resolution (FLOR) flux-adjusted model developed at

the Geophysical Fluid Dynamics Laboratory (Vecchi et al. 2014). FLOR has a high horizontal resolution of approximately 50km for the atmosphere (AM2.5) and land (LM3) components and a horizontal resolution of 1° (telescoping to 0.333° near the equator) for the ocean (MOM4) and sea ice (Sea Ice Simulator) components. It has a standard freely coupled version and a flux-adjusted version. The flux-adjustment in FLOR imposes fixed anomalous enthalpy, momentum and fresh water fluxes to the ocean to correct biases in the climatological seasonal cycle of SST, sea surface salinity and wind stress (against 1979-2012 observations). We use the flux-adjusted FLOR because of its much-improved mean climate and variability (see the next section).

Experiments are summarized in Table 1. We first introduce two long control simulations, one conducted with the fully coupled FLOR for 3500 years and the other with the uncoupled AM2.5 for 1000 years (note in AM2.5, the atmosphere is still coupled with the land). For simplicity, these control simulations are referred to as FLOR and AM2.5, respectively. Both simulations are driven by preindustrial level atmospheric composition and radiative forcing. In AM2.5, the boundary forcing is prescribed as the climatological annual cycle of monthly mean SST and sea ice (concentration and thickness) derived from the last 1000 years of FLOR. This 1000-year FLOR simulation is compared with AM2.5. FLOR and AM2.5 share the same radiative forcing and the same climatology at the surface, but differ in that the ocean (including sea ice) is fully active in FLOR but is replaced with an imposed climatological seasonal cycle of SST and sea ice in AM2.5. Precipitation variability in AM2.5 (excluding seasonal cycle) thus arises purely from internal atmosphere processes and coupling with land, while that in FLOR also includes contributions from the ocean (specifically, SST and sea ice variability). He et al. (2018a) showed that the ocean and atmosphere induced precipitation variability is linearly additive and that variability internal to the atmosphere (and land) can be cleanly extracted using atmosphere-only simulations with prescribed climatological SSTs. Analyzing and comparing the millennium-long fully coupled and atmosphere-only simulations allows for a physically clean and statistically robust assessment of the relative contributions of internal atmosphere processes and coupling with land versus the ocean in North American precipitation variability.

The remaining simulations are summarized in Table 1 and will be introduced later. We first examine the performance of the FLOR model in simulating North American precipitation and the associated climate variability in the tropics and midlatitudes, in order to build confidence

in using the model for investigating North American precipitation variability and the underlying atmospheric and oceanic processes.

2.2 Model performance

Precipitation biases over North America, especially over the western mountains, are a common problem in the current generation of climate models (Mejia et al. 2018). The FLOR model, however, substantially reduces these biases owing partly to its high resolution and flux adjustment. A recent paper by Johnson et al. (2020) has explained that the flux adjustment in FLOR reduces SST biases in the tropical Pacific and Atlantic, which improves the climatology of North American precipitation through atmosphere teleconnection mechanisms (including the ENSO teleconnection and those proposed by Kushnir et al. (2010)). Here we highlight the precipitation biases that remain in the flux-adjusted FLOR, against two observational products at 0.5° resolution, the Climatic Research Unit timeseries (CRU) datasets version 3.24.01 (Harris et al. 2014) and the Global Precipitation Climatology Centre (GPCC) version 2018 (Schneider et al. 2011). Fig. 1b shows that the flux-adjusted FLOR still has significant biases over most of North America, with too much precipitation over the Pacific Northwest and the monsoon region and too little precipitation over central to southeast North America. These positive biases are simulated throughout the year while the negative biases occur mainly during early summer to fall (Fig. 17 in appendix). Compared to the climatology, precipitation variability is better simulated in FLOR (Fig. 1c and Fig. 18 in appendix, indicated by more stippling). As will be shown later in the Results section, FLOR realistically simulates the leading modes of North American precipitation variability on seasonal and longer (up to the sampling length) time scales.

Tropical climate variability is assessed by comparing FLOR with the Met Office Hadley Centre's sea ice and sea surface temperature dataset (HadISST) version 1.1 (Rayner 2003). FLOR realistically simulates the spatial pattern and amplitude of tropical SST variability, although the ENSO variability is excessively strong in FLOR (Fig. 2a-b). This bias over the Niño3.4 occurs during February to June, while during the rest of the year FLOR simulates a very realistic Niño3.4 variability (Fig. 2c). FLOR also realistically simulates the ENSO spectrum, with a broad interannual peak consistent with observations (Fig. 2d) but seemingly too weak decadal variability.

To evaluate how FLOR simulates the ENSO teleconnection and impacts on North American precipitation, we compute the correlation coefficients between the Niño3.4 index and

SST, land precipitation and 200mb geopotential height (GHT200) during December to February (DJF). Observational fields include SST from HadISST, precipitation from CRU and geopotential height from the NOAA-CIRES-DOE Twentieth Century Reanalysis (20CR) version 2 (Compo et al. 2011) during 1901-2012. Fig. 3 shows that FLOR simulates the observed global ENSO teleconnection very well, indicated by the similar Rossby wave trains emanating from the tropical Pacific. Over the Pacific/North America sector, FLOR realistically simulates the observed PNA-like upper tropospheric circulation (GHT200) associated with ENSO (Fig. 3a vs 3c). In particular, observed correlations between North American precipitation and ENSO are realistically captured in FLOR, with a pattern of positive/negative correlations over southern/northern North America, respectively (Fig. 3b vs 3d). We note that the correlations appear a bit weaker in FLOR than in observations, which can be partly attributed to the uncertainty in the observed teleconnection patterns due to the insufficient sampling lengths (112 years, (Deser et al. 2017)).

To evaluate FLOR's performance in simulating midlatitude variability over the Pacific/North America sector (20°N-80°N, 100°E-50°W), we conduct an empirical orthogonal function (EOF) decomposition of monthly mean sea level pressure (SLP) variability and compare the leading modes between FLOR and the 20CR dataset (Fig. 4, top two rows). Clearly, FLOR faithfully simulates the top three EOF modes in terms of the spatial pattern and the explained variance. Accounting for about 24% of total variance in both FLOR and 20CR, the first EOF mode (EOF1) features three centers of action over the Aleutian Low, the Arctic Ocean and the Gulf Stream, respectively and likely reflects the surface expression of the PNA (which in literature is defined by middle to upper tropospheric geopotential heights). Note that EOF1 is nearly identical to the ENSO teleconnection pattern in SLP (black contours in Fig. 4 upper left two panels), suggesting that EOF1 is related to the ENSO variability. However, this EOF mode does not own its existence to ENSO, because it also appears as the first EOF mode in AM2.5 without the interactive varying ocean (Fig. 4 bottom left) and explains a similar amount of monthly SLP variance, 22.7% in AM2.5 vs 24.2% in FLOR. This result supports the familiar concept that ENSO affects the extratropics by projecting onto internal modes of atmospheric variability (e.g., Simmons et al. 1983; Palmer and Mansfield 1984; Geisler et al. 1985; Palmer 1993; Lau and Nath 1994; Saravanan 1998; Hoerling and Kumar 2002; Barsugli and Sardeshmukh 2002; Dai et al. 2017; Henderson et al. 2020). A similar story holds true for the

second and third EOF modes, with EOF2 being the North Pacific Oscillation (Walker 1924) and EOF3 being an east-west seesaw pattern over the Aleutian Islands. Both are realistically simulated in FLOR.

In summary, as shown by Johnson et al. (2020), the flux-adjusted high-resolution FLOR model substantially improves the simulation of North American precipitation climatology compared to its standard version and other peer models. Here we demonstrate that FLOR also realistically simulates climate variability both in the tropical oceans and midlatitudes as well as the ENSO teleconnection. Next, we move on to the focus of this work—North American precipitation variability on seasonal and longer time scales, evaluate how it is simulated in FLOR and investigate how it is shaped by atmospheric and oceanic processes.

3. Results

3.1 Dominant modes of variability in North American precipitation

To examine North American precipitation variability on seasonal and longer time scales, we focus on the dominant modes of variability in monthly precipitation calculated from an EOF decomposition. Note that the mean annual cycle has been removed from precipitation prior to the EOF decomposition. In observations and FLOR, the top two EOF modes are significantly separated from each other (and also other modes) based on the North test (North et al. 1982) and reflect the strong precipitation over the southeastern United States and the Pacific Northwest, respectively (recall Fig. 1a). In Fig. 5, for the first matching EOFs, both the observed and FLOR modes have the largest loading over the southeastern United States and explain about 9.0% and 7.8% of their total variance over North America, respectively. In Fig. 6, for the second matching EOFs, the observed and FLOR modes are dominated by two largest loadings along the Pacific Northwest and explains about 6.4% of the variance in observations and 8.8% in FLOR. The pattern correlation between observations and FLOR is 0.77 for the EOF modes in Fig. 5 and 0.87 in Fig. 6. Note that the order of the two modes is reversed between observations and FLOR, with the first (second) mode in observations being the second (first) mode in FLOR. The reversed order in FLOR is due to the relatively large biases in regions of strong precipitation, namely, the Pacific Northwest (more precipitation and larger variance, thus EOF 1) and the southeastern United States (less precipitation and weaker variance, thus EOF 2) (recall Fig. 1c). In addition to the spatial pattern, the principal components (PC) associated with these two EOF modes also

share similar behavior between observations and FLOR: their auto-correlation function decreases to almost zero at the 1-month lag (little or no persistence) and their spectrum is basically flat, both of which are characteristic of a white noise process. Overall, FLOR realistically simulates the spatial and spectral characteristics of the observed dominant modes of variability in monthly mean precipitation over North America. The reversed order of the two leading modes in FLOR and observations suggests that the relative contributions of the two leading modes to total precipitation variability are also reversed, which should be kept in mind for the rest of the paper.

AM2.5 without the interactive ocean simulates virtually the same top two EOF modes as the fully coupled FLOR (Fig. 5 and 6). For both EOF modes, the spatial structure is nearly identical between AM2.5 and FLOR with a pattern correlation of 0.99. The percentage of total variance explained by each EOF mode is also very similar, 8.5% (AM2.5) vs 8.8% (FLOR) for EOF 1 and 7.7% (AM2.5) vs 7.8% (FLOR) for EOF 2. The associated PCs exhibit little or no persistence and have a white-noise spectrum. These similarities suggest that the spatial and spectral characteristics of the two dominant modes of variability in monthly precipitation over North America are not sensitive to the ocean in the FLOR model and are determined by internal atmospheric dynamics and coupling with land.

In addition to monthly precipitation, we have conducted the same EOF decomposition on seasonal mean precipitation and low-pass-filtered monthly precipitation with various cutoff periods (1, 3 and 5 years) and also over various sub-regions of North America. These results are not shown but summarized here. Overall, the spatial pattern of leading EOF modes follows the pattern of strong precipitation (as expected, because strong precipitation implies strong variance and the EOF decomposition by design maximizes the variance explained by the leading modes). The main quantitative difference from the results based on monthly precipitation is in the percentage of explained variance, which increases by various extents depending on the season and the sub-region. However, regardless of seasons and sub-regions, the leading EOF modes of FLOR and AM2.5 still share very similar spatial patterns and white-noise behavior. These similarities further suggest that internal atmospheric dynamics and coupling with land dominate the spatial and spectral characteristics of the leading modes of precipitation variability over North America not only on high-frequency time scales (in monthly precipitation) but also on low-frequency (interannual to decadal) time scales. Next, we return to monthly fields and present the physical processes associated with the two leading EOF modes.

To examine the large-scale atmosphere circulation and possible SST anomalies associated with the top two EOF modes, we calculate the correlation coefficients between the associated PCs and SLP, GHT200 and surface temperature. For the EOF mode with a strong loading over the southeastern United States (Fig. 5), the associated large-scale atmosphere circulation is very similar over North America (where the EOF analysis is performed, indicated by the magenta box in each panel) among observations, FLOR and AM2.5. In Fig. 7, the large-scale pattern of SLP correlation (contours in top row) includes two anticyclones centered around east of the Caribbean and off the Canada-Alaska coast and one cyclone in between over the U.S.. The GHT200 correlation (shading in bottom row) exhibits a similar pattern (but slightly tilted westward), suggesting an equivalent barotropic structure for the associated circulation over North America. The implied geostrophic winds and moisture advection are consistent with the EOF precipitation anomalies. In particular, the moist southerlies from the Gulf of Mexico support the strong precipitation over the southeastern United States, while the wet-dry dipole along the Pacific Northwest (weak in observations but strong in the model simulations) agrees with the wet oceanic southerlies and dry inland northerlies that straddle the anticyclone there.

For the correlation with surface temperature, the local patterns over North America are also very similar among observations, FLOR and AM2.5, and largely consistent with the anomalous advection of mean surface temperature (that is, southerlies lead to warming and vice visa). Remotely over the ocean, the pattern of SST correlation is similar between observations and FLOR (AM2.5 has no SST variability by design). In particular, the EOF mode shown in Fig. 5 is accompanied with positive SST (also increased GHT200 aloft) anomalies over the tropical Pacific and Indian Ocean, suggesting a role for the tropical oceans. However, the weak magnitude of the correlation implies that the role of the tropical oceans is very limited for the variability in monthly precipitation over North America. AM2.5 without the interactive ocean simulates the associated surface temperature and atmospheric circulation over North America (and actually has opposite sign GHT200 anomalies in the tropics), suggesting that the physical processes underlying the precipitation EOF mode shown in Fig. 5 can arise solely from internal atmosphere dynamics and coupling with land.

Similar conclusions are found for the EOF mode shown in Fig. 6 reflecting strong precipitation anomalies over the Pacific coast of North America. In Fig. 8, the associated atmosphere circulation over North America features a strong equivalent-barotropic anticyclone

over the Pacific Northwest in observations, FLOR and AM2.5. To the west of the anticyclone, the associated geostrophic southerlies bring warm moist air from the ocean to British Columbia and Alaska. To the south of the anticyclone geostrophic easterlies bring cold dry air from inland to the US west coast. This results in the dipole pattern in both surface temperature (Fig. 8, shading in top row) and precipitation (Fig. 6). Note that the anticyclone is part of an anomalous circulation that reflects changes in the strength of midlatitude stationary eddies (Fig. 8, contours in bottom row). This EOF mode also exhibits some positive but weak correlations with tropical SSTs, mostly in FLOR. We note that the large-scale atmosphere circulation associated with the two leading EOF modes has three centers of actions over the North Pacific/American sector. These centers of action resemble but are shifted relative to those of the PNA (the upper left two panels in Fig. 4). This difference in atmosphere circulation is consistent with the fact that both of the leading EOF modes in precipitation are different from the precipitation pattern associated with the PNA (not shown but is nearly identical to the ENSO teleconnection pattern in Fig. 3).

Overall, despite the reversed order of the two leading EOF modes, FLOR faithfully reproduces the spatial and spectral features of the observed dominant variability in monthly precipitation over North America and the associated large-scale atmosphere circulation and surface temperature. Comparing the fully coupled FLOR and AM2.5 without the interactive ocean, we find that their dominant modes of monthly (and seasonal) precipitation variability over North America have nearly identical spatial structures, explained fraction of total variance, spectral behavior (no persistence and white-noise spectrum) and the associated large-scale atmosphere circulation and local surface temperature anomalies. These similarities suggest that the dominant variability in North American precipitation arises from internal atmosphere dynamics and coupling with land, and does not require SST variability to exist. However, SST variability, particularly in the tropics, still affects North American precipitation, as demonstrated in the literature and indicated here by the positive correlation with tropical SSTs in FLOR and observations. The weak magnitude of correlation suggests that the impacts of the tropical oceans are very limited. The results that the ocean does not change the spatial and spectral characteristics of North American precipitation leading modes of variability suggest that SST variability does not create its own modes of atmosphere variability but rather excites modes of variability that already exist in the atmosphere. This interpretation is also supported by the results in Fig. 4, where the leading mode of midlatitude variability in AM2.5 without the

interactive ocean is nearly identical to the ENSO teleconnection pattern in the fully coupled FLOR and observations. Note that these results are consistent with the familiar concept that SST variability affects the atmosphere by projecting onto internal modes of atmospheric variability. We emphasize here that SST variability does not significantly change the basic characteristics of the large-scale atmospheric variability and its influence only accounts for a small portion of the total North America precipitation variability. Despite its limited impacts, SST variability is still the main source of long-term predictability for North American precipitation variability beyond the time scales of internal atmosphere dynamics.

3.2 Precipitation variance over SWNA

To quantify the impacts of the ocean on year-to-year variance of precipitation over North America, we compute the fractional change of monthly precipitation standard deviation at each grid point for each calendar month between FLOR and AM2.5 by

$$\frac{STD_{FLOR}-STD_{AM2.5}}{STD_{FLOR}} \times 100\%,$$

where STD_{FLOR} and $STD_{AM2.5}$ are the year-to-year standard deviation of monthly precipitation evaluated at the same grid point for the same calendar month in FLOR and AM2.5, respectively. In Fig. 9, the impacts of the ocean on precipitation variance are not significant (at 1% level) for most of North America throughout the year. The largest significant fractional increase of precipitation variance due to the ocean occurs over southwest North America (SWNA) during May to about September, with magnitudes up to 90% over parts of SWNA especially the North American monsoon region during June and July. In contrast, during winter (November to February) when ENSO variability peaks (recall Fig. 2c), the fractional increase of precipitation variance is relatively weak and only significant over smaller areas of SWNA.

How does the ocean amplify precipitation variance over SWNA during the late spring through summer? To answer this question, we examine the factors that affect precipitation variability, including evaporation and atmospheric moisture convergence. The latter depends on circulation and moisture variability, which we will focus on. Similar to precipitation, we compute the fractional change in year-to-year standard deviation of these two factors between FLOR and AM2.5. The metrics used are monthly 500mb pressure velocity (Omega500) and column-integrated water vapor (CWV) content. Over SWNA, no systematic significant changes are found in the standard deviation of monthly Omega500 between FLOR and AM2.5 throughout the year (Fig. 10), which suggests that the interactive ocean in FLOR does not

414 significantly affect the variance of atmosphere divergent circulation over SWNA. In contrast, the
415 standard deviation in CWV is significantly enhanced over SWNA during May to about October
416 (Fig. 11), similar to the changes in precipitation standard deviation (Fig. 9). Together these
417 results suggest that the amplified precipitation variance over SWNA in FLOR relative to AM2.5
418 is caused by the enhanced variability in atmosphere moisture content.
419 How does the interactive ocean enhance CWV variability over SWNA and why is this
420 enhancement mainly during late spring to summer but not winter? Our interpretation is that the
421 seasonal mean atmosphere circulation is transporting enhanced CWV anomalies from
422 surrounding oceans into SWNA. This is supported in FLOR by the vertically-integrated fluxes of
423 specific humidity standard deviation by mean winds, $\int \bar{\vec{u}} \cdot STD(q')dp$, where $\bar{\vec{u}}$ is climatological
424 monthly winds, $STD(q')$ is the standard deviation of monthly specific humidity anomalies and
425 the integral is done for the entire atmosphere. This quantity can also be interpreted as the
426 vertically-integrated mean circulation weighted by moisture variability and thus reflects the
427 mean circulation of the lower troposphere where most of the moisture is. During late spring to
428 early fall (around May to October), CWV variability is significantly enhanced by SST variability
429 over the tropical to midlatitude North Pacific, which extends northeastward into the SWNA
430 region following the mean southwesterly winds (see vectors in Fig. 11). In contrast, during
431 winter (around December to March), the enhanced CWV variability over the northeastern Pacific
432 is confined to the subtropics (presumably owing to the colder atmosphere and smaller moisture
433 capacity in winter) and the mean northwesterly winds are from ocean regions where CWV
434 variability appears insensitive to SST variability, both of which are unfavorable to enhance CWV
435 variability over SWNA.
436 Which parts of the ocean are responsible for the intensification of precipitation variability
437 over SWNA? To answer this question, we conduct additional experiments (Table 1) that are
438 similar to the AM2.5 simulation but with time varying monthly SSTs from FLOR imposed in
439 different oceans during different times (note that these experiments have first been reported in a
440 companion study focusing on synoptic extreme precipitation in June over SWNA (Zhang 2020)).
441 Four experiments are conducted, each 600 years long (corresponding to FLOR 2601-3200). The
442 first one has monthly SSTs prescribed over the entire globe (for all months, hereafter, Globe_1-
443 12) to test whether this technique (AM2.5 imposed with monthly SSTs) can reproduce the FLOR
444 precipitation variance over SWNA given that interactive ocean-atmosphere coupling may matter

(e.g., Bretherton and Battisti 2000; He et al. 2017, 2018b). The other three have monthly SSTs prescribed between 35°N and 35°S (with a 5° linear buffer zone) in the entire tropics for all months (Tropic_1-12), the tropical Pacific for October to May (Pacific_10-5) and the tropical Atlantic for May to October (Atlantic_5-10), respectively. The reason for prescribing SSTs in Pacific_10-5 and Atlantic_5-10 only during the stated months is that SST correlations with the SWNA precipitation are only significant during the stated months over the respective ocean basins (Fig. 19 in appendix). Tropic_1-12 can test the role of SSTs in the tropics versus extratropics, while Pacific_10-5 and Atlantic_5-10 can test the role of SSTs in the tropical Pacific from October to May and in the tropical Atlantic from May to October, respectively. We note that, in Pacific_10-5 and Atlantic_5-10, the May and October SSTs are extrapolated into their neighbor months such that September and June in Pacific_10-5 and April and November in Atlantic_5-10 also have anomalous SST forcing (by default in all AM2.5 simulations, monthly SST values are placed in the middle of each month before interpolation onto the model time step). These four experiments allow us to identify the oceans responsible for the amplification of precipitation variance over SWNA.

Compared to AM2.5 without the interactive ocean, Globe_1-12 generally well reproduces the month-to-month variance (i.e., average of the year-to-year variance over twelve calendar months) of both precipitation and CWV over SWNA in FLOR, albeit a bit weaker and confined to lower latitudes (Fig. 12a-d). These similarities also hold true for the year-to-year variance (Fig. 20-21 in appendix), which justifies the experimental technique to pin down the oceans responsible for the enhanced precipitation variance over SWNA in FLOR. Tropic_1-12 without extratropical SST variability also well reproduces the precipitation and CWV variance over SWNA in FLOR (Fig. 12e-f for month-to-month variance and Fig. 22-23 for year-to-year variance), suggesting that the tropical SST variability is responsible for the enhanced precipitation variance over SWNA in FLOR.

For the total month-to-month variability, Pacific_10-5 (Fig. 12g-h) is able to enhance the variance in both CWV and precipitation over most of SWNA, while Atlantic_5-10 (Fig. 12i-j) only enhances the CWV variance locally in the tropical Atlantic but neither the CWV nor the precipitation variance over SWNA (except southern Mexico and northern central America). For the year-to-year variability, Pacific_10-5 enhances the precipitation (Fig. 13) and CWV (Fig. 14) variance over SWNA mainly during May and June (recall the extrapolation of SST forcing from

May to June), similar to the enhancement in FLOR, Globe_1-12 and Tropic_1-12. In contrast, Atlantic_5-10 does not simulate systematic enhancement of precipitation (Fig. 15) and CWV (Fig. 16) variance over SWNA during May to October when the SST forcing is imposed in the tropical Atlantic. Together, these results suggest that it is the tropical Pacific that accounts for the enhanced precipitation variance over SWNA in FLOR relative to AM2.5.

The lack of impacts from the tropical Atlantic on the SWNA precipitation variance seems inconsistent with previous studies (Kushnir et al. 2010; Johnson et al. 2020). In particular, Johnson et al. (2020) have attributed most of the climatological precipitation biases over southern North America in the standard FLOR model to the strong SST biases in the tropical North Atlantic. This paradox can be explained by the different magnitudes of SST biases and variability in the tropical North Atlantic relative to the tropical Pacific. The SST biases in the standard FLOR model are much larger in the tropical North Atlantic (about 1-3K) than the tropical Pacific (less than 1K, see Fig. 2 in Johnson et al.), while the total month-to-month variability in the flux-adjusted FLOR is much stronger in the tropical Pacific than the tropical Atlantic (Fig. 2b). Therefore, our results from Atlantic_5-10 should be interpreted as that SST variability in the tropical Atlantic is relatively weak and unable to significantly affect the variance of atmosphere moisture content and thus precipitation over SWNA. The enhancement of the SWNA precipitation variance in FLOR relative to AM2.5 is mainly caused by the tropical Pacific through the new mechanism proposed in this work.

We point out an important distinction between our new mechanism and the classic ENSO teleconnection mechanism. In the ENSO teleconnection mechanism, tropical Pacific SST anomalies drive anomalous atmosphere circulation over SWNA that is capable of inducing anomalous precipitation. Our mechanism does not directly involve changes in atmosphere circulation over SWNA, but only involve enhanced atmosphere moisture content variability, that is, larger atmosphere moisture content anomalies. A new implication from our mechanism is that an interactive ocean is crucial to simulate and predict the amplitude of precipitation variability (i.e., precipitation intensity) over SWNA.

4. Summary and Discussion

We have quantified the atmospheric and oceanic contributions to North American precipitation variability on seasonal and longer time scales in the FLOR model. FLOR features a

50km resolution in its atmosphere/land components and flux adjustment to correct biases in mean SST; as a result, it greatly reduces the pervasive biases in North American precipitation that have plagued climate models of the same generation. FLOR also realistically simulates tropical and midlatitude climate variability as well as the ENSO teleconnection, all of which are critical for a reliable quantification of the atmospheric and oceanic contributions to North American precipitation variability.

Comparing two millennium-long simulations with and without an active ocean (FLOR and AM2.5), we find that the dominant modes of variability in North American monthly precipitation between the two simulations share a nearly identical spatial structure, explained fraction of total variance and white-noise spectra with no persistence. Furthermore, the associated large-scale atmosphere circulation and surface temperature anomalies over North America are also very similar in terms of both spatial pattern and magnitude. These similarities suggest that the dominant modes of North American precipitation variability do not owe their existence to the ocean, but rather arise from internal atmosphere processes and coupling with land.

In the fully coupled FLOR, however, the dominant modes of North American precipitation variability are still significantly correlated with the tropical oceans, especially the tropical Pacific and Indian Oceans. These correlations are consistent with observations and previous studies that have demonstrated a role for the tropical oceans. How the tropical oceans affect extratropical climate variability has been long debated, with some arguing that tropical variability exerts its own unique impacts by driving atmospheric circulation anomalies that are distinct from internal modes of atmospheric variability (e.g., Straus and Shukla 2000) but others arguing that tropical variability merely excites modes of variability that already exist in the atmosphere (e.g., Simmons et al. 1983; Palmer and Mansfield 1984; Geisler et al. 1985; Palmer 1993; Lau and Nath 1994; Saravanan 1998; Hoerling and Kumar 2002; Barsugli and Sardeshmukh 2002; Dai et al. 2017; Henderson et al. 2020). Here our results on North American precipitation variability support the latter argument. In particular, the ENSO teleconnection pattern over the Pacific/North America sector in FLOR appears in AM2.5 without the interactive ocean as the leading mode of midlatitude variability. This corroborates the idea that tropical climate variability affects the extratropics by exciting modes of variability that already exist in the atmosphere. Taken together, our modeling results suggest that internal atmosphere dynamics

and coupling with land determine the spatial and spectral characteristics of the leading modes of North American precipitation variability and dictate their explained fraction of total variance, while the tropical oceans contribute by exciting the same atmosphere dynamical processes.

Although the tropical oceans do not change the spatial and spectral characteristics of the leading modes of precipitation variability over the entire North America, they significantly enhance the variance of monthly precipitation over SWNA in FLOR relative to AM2.5. This enhancement in FLOR is seasonal and occurs mainly during late spring through summer when the ENSO variability is weakest (Fig. 2) and the correlation between the tropical Pacific SST and SWNA precipitation is weak or not significant (Fig. 19 in appendix). Examining the two factors critical for land precipitation, we find significant enhancement in the variance of atmosphere moisture content but not of divergent circulation over SWNA. The enhanced variability of atmosphere moisture content over SWNA is traced down to the tropical Pacific, where SST variability amplifies atmosphere moisture content variability, which is then transported into the SWNA region during late spring to summer by the seasonal mean southwesterly winds. This interpretation is different from the classic ENSO teleconnection mechanism not only in that it operates mainly during non-ENSO seasons, but more importantly, because it involves a different pathway of influence from the northeastern tropical Pacific to SWNA that is associated with the mean circulation and moisture anomalies as opposed to the dominance of anomalous circulation in the classic ENSO teleconnection mechanism. Therefore, our interpretation is a new mechanism, in addition to the classic ENSO teleconnection, via which the tropical Pacific Ocean variability affects precipitation over SWNA. Note that this mechanism has been invoked in a companion study (Zhang 2020) to explain how the tropical Pacific intensifies extreme rainfall over parts of SWNA in June. Here we extend the mechanism from synoptic time scales to seasonal and longer time scales.

We point out that the amplification of the SWNA precipitation variability by the tropical oceans has been noted by Seager et al. (2014, see their Fig. 5 and the relevant discussions), but their presumed interpretation is the classic ENSO teleconnection. In addition, projected future amplification in hydroclimate variability (Seager et al. 2011; Pendergrass et al. 2017) has been attributed to global warming-induced increases in *mean* atmosphere moisture content via the thermodynamic Clausius-Clapeyron relationship. Our work differs from those projection studies in that we focus on internal climate variability for a constant radiative forcing with a steady

atmosphere moisture content climatology. The variability in atmosphere moisture content (over the ocean) comes mostly from a dynamical redistribution (i.e., convergence or divergence) of atmosphere moisture induced by SST variability.

SST variability in the tropical Atlantic does not significantly contribute to the amplification of precipitation variance over SWNA (except for southern Mexico and northern central America), in contrast to previous studies demonstrating a role for the tropical North Atlantic. This paradox is likely attributed to the weak amplitude of the tropical Atlantic SST variability, which is unable to enhance the variance of atmosphere moisture content over SWNA. We emphasize that the tropical Atlantic SST variability can still affect the precipitation variability over SWNA through other dynamical processes (Kushnir et al. 2010; Johnson et al. 2020).

The contributions of atmospheric and oceanic processes to North American precipitation variability on seasonal and longer time scales in FLOR are summarized as follows. The spatial and spectral characteristics of the dominant modes of variability in North American monthly (and seasonal) precipitation along with their explained fraction of total variance are controlled by internal atmosphere processes and coupling with land. Ocean variability, mainly from the tropical oceans, contributes to North American precipitation variability in two ways. First, on continental scales, it dynamically excites the same internal atmosphere processes as above (to some extent, as beating a drum excites its normal modes), and thus does not change the spatial characteristics of the leading modes. This impact is secondary compared to internal atmosphere processes and unable to significantly modify the leading modes' white-noise spectrum and explained fraction of total variance. Nonetheless, this ocean impact provides potential long-term predictability for North American precipitation beyond the timescales limited by internal atmosphere processes. Second, on regional scales, SST variability in the tropical Pacific amplifies atmosphere moisture content variability, which during late spring to summer is transported by mean southwesterly winds into the SWNA region and enhances the variance of precipitation over SWNA. This enhancement implies that the tropical Pacific is required for a reliable simulation and prediction of the intensity of precipitation over SWNA.

Acknowledgement

This work is supported by NSF awards OCE-16-57209 and AGS-19-34363. Discussions with Tom Delworth are much appreciated. Comments from three anonymous reviewers help clarify some overlooked issues. GPCC Precipitation data and NOAA-CIRES-DOE Twentieth Century reanalysis products are provided by the NOAA/OAR/ESRL PSD, Boulder, Colorado, USA, from their Web site at https://www.esrl.noaa.gov/psd/. All modeling data used here will be available upon request.

References

Barsugli JJ, Sardeshmukh PD (2002) Global Atmospheric Sensitivity to Tropical SST Anomalies throughout the Indo-Pacific Basin. J Climate 15:3427–3442. https://doi.org/10.1175/1520-0442(2002)015<3427:GASTTS>2.0.CO;2

Bates GT, Hoerling MP, Kumar A (2001) Central U.S. Springtime Precipitation Extremes: Teleconnections and Relationships with Sea Surface Temperature. J Climate 14:3751–3766. https://doi.org/10.1175/1520-0442(2001)014<3751:CUSSPE>2.0.CO;2

Bjerknes J (1966) A possible response of the atmospheric Hadley circulation to equatorial anomalies of ocean temperature. Tellus 18:820–829. https://doi.org/10.1111/j.2153-3490.1966.tb00303.x

Bjerknes J (1969) ATMOSPHERIC TELECONNECTIONS FROM THE EQUATORIAL PACIFIC. Mon Wea Rev 97:163–172. https://doi.org/10.1175/1520-0493(1969)097<0163:ATFTEP>2.3.CO;2

Bretherton CS, Battisti DS (2000) An interpretation of the results from atmospheric general circulation models forced by the time history of the observed sea surface temperature distribution. Geophys Res Lett 27:767–770. https://doi.org/10.1029/1999GL010910

Castro CL, McKee TB, Pielke RA (2001) The Relationship of the North American Monsoon to Tropical and North Pacific Sea Surface Temperatures as Revealed by Observational Analyses. Journal of Climate 14:4449–4473. https://doi.org/10.1175/1520-0442(2001)014<4449:TROTNA>2.0.CO;2

Chen P, Newman M (1998) Rossby Wave Propagation and the Rapid Development of Upper-Level Anomalous Anticyclones during the 1988 U.S. Drought. J Climate 11:2491–2504. https://doi.org/10.1175/1520-0442(1998)011<2491:RWPATR>2.0.CO;2

Chen Z, Gan B, Wu L, Jia F (2018) Pacific-North American teleconnection and North Pacific Oscillation: historical simulation and future projection in CMIP5 models. Clim Dyn 50:4379–4403. https://doi.org/10.1007/s00382-017-3881-9

632 Compo GP, Whitaker JS, Sardeshmukh PD, et al (2011) The Twentieth Century Reanalysis
633 Project. Quarterly Journal of the Royal Meteorological Society 137:1–28.
634 https://doi.org/10.1002/qj.776

635 Cook BI, Miller RL, Seager R (2009) Amplification of the North American "Dust Bowl" drought
636 through human-induced land degradation. PNAS 106:4997–5001.
637 https://doi.org/10.1073/pnas.0810200106

638 Cook BI, Seager R, Miller RL (2011) Atmospheric circulation anomalies during two persistent
639 north american droughts: 1932–1939 and 1948–1957. Clim Dyn 36:2339–2355.
640 https://doi.org/10.1007/s00382-010-0807-1

641 Dai Y, Feldstein SB, Tan B, Lee S (2017) Formation Mechanisms of the Pacific–North American
642 Teleconnection with and without Its Canonical Tropical Convection Pattern. J Climate
643 30:3139–3155. https://doi.org/10.1175/JCLI-D-16-0411.1

644 Deser C, Simpson IR, McKinnon KA, Phillips AS (2017) The Northern Hemisphere Extratropical
645 Atmospheric Circulation Response to ENSO: How Well Do We Know It and How Do We
646 Evaluate Models Accordingly? J Climate 30:5059–5082. https://doi.org/10.1175/JCLI-D-
647 16-0844.1

648 Enfield DB, Mestas-Nuñez AM, Trimble PJ (2001) The Atlantic Multidecadal Oscillation and its
649 relation to rainfall and river flows in the continental U.S. Geophysical Research Letters
650 28:2077–2080. https://doi.org/10.1029/2000GL012745

651 Geisler JE, Blackmon ML, Bates GT, Muñoz S (1985) Sensitivity of January Climate Response to
652 the Magnitude and Position of Equatorial Pacific Sea Surface Temperature Anomalies. J
653 Atmos Sci 42:1037–1049. https://doi.org/10.1175/1520-
654 0469(1985)042<1037:SOJCRT>2.0.CO;2

655 Harris I, Jones P d., Osborn T j., Lister D h. (2014) Updated high-resolution grids of monthly
656 climatic observations – the CRU TS3.10 Dataset. Int J Climatol 34:623–642.
657 https://doi.org/10.1002/joc.3711

658 He J, Deser C, Soden BJ (2017) Atmospheric and Oceanic Origins of Tropical Precipitation
659 Variability. J Climate 30:3197–3217. https://doi.org/10.1175/JCLI-D-16-0714.1

660 He J, Johnson NC, Vecchi GA, et al (2018a) Precipitation Sensitivity to Local Variations in
661 Tropical Sea Surface Temperature. Journal of Climate 31:9225–9238.
662 https://doi.org/10.1175/JCLI-D-18-0262.1

663 He J, Kirtman B, Soden BJ, et al (2018b) Impact of Ocean Eddy Resolution on the Sensitivity of
664 Precipitation to CO2 Increase. Geophysical Research Letters 45:7194–7203.
665 https://doi.org/10.1029/2018GL078235

Henderson SA, Vimont DJ, Newman M (2020) The Critical Role of Non-Normality in Partitioning Tropical and Extratropical Contributions to PNA Growth. J Climate 33:6273–6295. https://doi.org/10.1175/JCLI-D-19-0555.1

Herweijer C, seager richard, Cook ER (2006) North American droughts of the mid to late nineteenth century: a history, simulation and implication for Mediaeval drought. The Holocene

Hoerling M, Kumar A (2003) The Perfect Ocean for Drought. Science 299:691–694. https://doi.org/10.1126/science.1079053

Hoerling M, Quan X-W, Eischeid J (2009) Distinct causes for two principal U.S. droughts of the 20th century. Geophysical Research Letters 36:. https://doi.org/10.1029/2009GL039860

Hoerling MP, Kumar A (1997) Why do North American climate anomalies differ from one El Niño event to another? Geophysical Research Letters 24:1059–1062. https://doi.org/10.1029/97GL00918

Hoerling MP, Kumar A (2002) Atmospheric Response Patterns Associated with Tropical Forcing. J Climate 15:2184–2203. https://doi.org/10.1175/1520-0442(2002)015<2184:ARPAWT>2.0.CO;2

Horel JD, Wallace JM (1981) Planetary-Scale Atmospheric Phenomena Associated with the Southern Oscillation. Monthly Weather Review 109:813–829. https://doi.org/10.1175/1520-0493(1981)109<0813:PSAPAW>2.0.CO;2

Hoskins BJ, Karoly DJ (1981) The Steady Linear Response of a Spherical Atmosphere to Thermal and Orographic Forcing. J Atmos Sci 38:1179–1196. https://doi.org/10.1175/1520-0469(1981)038<1179:TSLROA>2.0.CO;2

Johnson NC, Krishnamurthy L, Wittenberg AT, et al (2020) The Impact of Sea Surface Temperature Biases on North American Precipitation in a High-Resolution Climate Model. J Climate 33:2427–2447. https://doi.org/10.1175/JCLI-D-19-0417.1

Kumar A, Chen M (2020) Understanding Skill of Seasonal Mean Precipitation Prediction over California during Boreal Winter and Role of Predictability Limits. J Climate 33:6141–6163. https://doi.org/10.1175/JCLI-D-19-0275.1

Kushnir Y, Seager R, Ting M, et al (2010) Mechanisms of Tropical Atlantic SST Influence on North American Precipitation Variability. J Climate 23:5610–5628. https://doi.org/10.1175/2010JCLI3172.1

Lau N-C, Nath MJ (1994) A Modeling Study of the Relative Roles of Tropical and Extratropical SST Anomalies in the Variability of the Global Atmosphere-Ocean System. J Climate 7:1184–1207. https://doi.org/10.1175/1520-0442(1994)007<1184:AMSOTR>2.0.CO;2

Leathers DJ, Yarnal B, Palecki MA (1991) The Pacific/North American Teleconnection Pattern and United States Climate. Part I: Regional Temperature and Precipitation Associations. Journal of Climate 4:517–528. https://doi.org/10.1175/1520-0442(1991)004<0517:TPATPA>2.0.CO;2

Linkin ME, Nigam S (2008) The North Pacific Oscillation–West Pacific Teleconnection Pattern: Mature-Phase Structure and Winter Impacts. Journal of Climate 21:1979–1997. https://doi.org/10.1175/2007JCLI2048.1

Liu AZ, Ting M, Wang H (1998) Maintenance of Circulation Anomalies during the 1988 Drought and 1993 Floods over the United States. J Atmos Sci 55:2810–2832. https://doi.org/10.1175/1520-0469(1998)055<2810:MOCADT>2.0.CO;2

Liu Z, Tang Y, Jian Z, et al (2017) Pacific North American circulation pattern links external forcing and North American hydroclimatic change over the past millennium. PNAS 114:3340–3345. https://doi.org/10.1073/pnas.1618201114

Lyon B, Dole RM (1995) A Diagnostic Comparison of the 1980 and 1988 U.S. Summer Heat Wave-Droughts. J Climate 8:1658–1675. https://doi.org/10.1175/1520-0442(1995)008<1658:ADCOTA>2.0.CO;2

McCabe GJ, Palecki MA, Betancourt JL (2004) Pacific and Atlantic Ocean influences on multidecadal drought frequency in the United States. PNAS 101:4136–4141. https://doi.org/10.1073/pnas.0306738101

Mejia JF, Koračin D, Wilcox EM (2018) Effect of coupled global climate models sea surface temperature biases on simulated climate of the western United States. International Journal of Climatology 38:5386–5404. https://doi.org/10.1002/joc.5817

North GR, Bell TL, Cahalan RF, Moeng FJ (1982) Sampling Errors in the Estimation of Empirical Orthogonal Functions. Mon Wea Rev 110:699–706. https://doi.org/10.1175/1520-0493(1982)110<0699:SEITEO>2.0.CO;2

Palmer TN (1993) Extended-Range Atmospheric Prediction and the Lorenz Model. Bull Amer Meteor Soc 74:49–65. https://doi.org/10.1175/1520-0477(1993)074<0049:ERAPAT>2.0.CO;2

Palmer TN, Branković Č (1989) The 1988 US drought linked to anomalous sea surface temperature. Nature 338:54–57. https://doi.org/10.1038/338054a0

Palmer TN, Mansfield DA (1984) Response of two atmospheric general circulation models to sea-surface temperature anomalies in the tropical East and West Pacific. Nature 310:483–485. https://doi.org/10.1038/310483a0

Palmer TN, Mansfield DA (1986) A study of wintertime circulation anomalies during past El Niño events using a high resolution general circulation model. I: Influence of model

735 climatology. Quarterly Journal of the Royal Meteorological Society 112:613–638.
736 https://doi.org/10.1002/qj.49711247304

737 Pendergrass AG, Knutti R, Lehner F, et al (2017) Precipitation variability increases in a warmer
738 climate. Scientific Reports 7:1–9. https://doi.org/10.1038/s41598-017-17966-y

739 Rasmusson EM, Wallace JM (1983) Meterological Aspects of the El Niño/Southern Oscillation.
740 Science, New Series 222:1195–1202

741 Rayner NA (2003) Global analyses of sea surface temperature, sea ice, and night marine air
742 temperature since the late nineteenth century. J Geophys Res 108:4407.
743 https://doi.org/10.1029/2002JD002670

744 Ropelewski CF, Halpert MS (1986) North American Precipitation and Temperature Patterns
745 Associated with the El Niño/Southern Oscillation (ENSO). Mon Wea Rev 114:2352–2362.
746 https://doi.org/10.1175/1520-0493(1986)114<2352:NAPATP>2.0.CO;2

747 Ruprich-Robert Y, Delworth T, Msadek R, et al (2018) Impacts of the Atlantic Multidecadal
748 Variability on North American Summer Climate and Heat Waves. J Climate 31:3679–
749 3700. https://doi.org/10.1175/JCLI-D-17-0270.1

750 Ruprich-Robert Y, Msadek R, Castruccio F, et al (2016) Assessing the Climate Impacts of the
751 Observed Atlantic Multidecadal Variability Using the GFDL CM2.1 and NCAR CESM1
752 Global Coupled Models. J Climate 30:2785–2810. https://doi.org/10.1175/JCLI-D-16-
753 0127.1

754 Saravanan R (1998) Atmospheric Low-Frequency Variability and Its Relationship to Midlatitude
755 SST Variability: Studies Using the NCAR Climate System Model. J Climate 11:1386–1404.
756 https://doi.org/10.1175/1520-0442(1998)011<1386:ALFVAI>2.0.CO;2

757 Schneider U, Becker A, Finger, Peter, et al (2011) GPCC Full Data Reanalysis Version 6.0 at 0.5°:
758 Monthly Land-Surface Precipitation from Rain-Gauges built on GTS-based and Historic
759 Data. https://doi.org/10.5676/DWD_GPCC/FD_M_V7_050

760 Schubert S, Gutzler D, Wang H, et al (2009) A U.S. CLIVAR Project to Assess and Compare the
761 Responses of Global Climate Models to Drought-Related SST Forcing Patterns: Overview
762 and Results. J Climate 22:5251–5272. https://doi.org/10.1175/2009JCLI3060.1

763 Schubert SD, Suarez MJ, Pegion PJ, et al (2004a) Causes of Long-Term Drought in the U.S. Great
764 Plains. J Climate 17:485–503. https://doi.org/10.1175/1520-
765 0442(2004)017<0485:COLDIT>2.0.CO;2

766 Schubert SD, Suarez MJ, Pegion PJ, et al (2004b) On the Cause of the 1930s Dust Bowl. Science
767 303:1855–1859. https://doi.org/10.1126/science.1095048

768 Seager R, Harnik N, Kushnir Y, et al (2003) Mechanisms of Hemispherically Symmetric Climate
769 Variability. J Climate 16:2960–2978. https://doi.org/10.1175/1520-
770 0442(2003)016<2960:MOHSCV>2.0.CO;2

771 Seager R, Harnik N, Robinson WA, et al (2005a) Mechanisms of ENSO-forcing of hemispherically
772 symmetric precipitation variability. Quarterly Journal of the Royal Meteorological
773 Society 131:1501–1527. https://doi.org/10.1256/qj.04.96

774 Seager R, Hoerling M (2014) Atmosphere and Ocean Origins of North American Droughts. J
775 Climate 27:4581–4606. https://doi.org/10.1175/JCLI-D-13-00329.1

776 Seager R, Kushnir Y, Herweijer C, et al (2005b) Modeling of Tropical Forcing of Persistent
777 Droughts and Pluvials over Western North America: 1856–2000. J Climate 18:4065–
778 4088. https://doi.org/10.1175/JCLI3522.1

779 Seager R, Naik N, Vogel L (2011) Does Global Warming Cause Intensified Interannual
780 Hydroclimate Variability? J Climate 25:3355–3372. https://doi.org/10.1175/JCLI-D-11-
781 00363.1

782 Seager R, Ting M (2017) Decadal Drought Variability Over North America: Mechanisms and
783 Predictability. Curr Clim Change Rep 1–9. https://doi.org/10.1007/s40641-017-0062-1

784 Simmons AJ, Wallace JM, Branstator GW (1983) Barotropic Wave Propagation and Instability,
785 and Atmospheric Teleconnection Patterns. J Atmos Sci 40:1363–1392.
786 https://doi.org/10.1175/1520-0469(1983)040<1363:BWPAIA>2.0.CO;2

787 Stevenson S, Timmermann A, Chikamoto Y, et al (2014) Stochastically Generated North
788 American Megadroughts. J Climate 28:1865–1880. https://doi.org/10.1175/JCLI-D-13-
789 00689.1

790 Straus DM, Shukla J (2000) Distinguishing between the SST-forced variability and internal
791 variability in mid latitudes: Analysis of observations and GCM simulations. Quarterly
792 Journal of the Royal Meteorological Society 126:2323–2350.
793 https://doi.org/10.1002/qj.49712656716

794 Suarez MJ (1985) Chapter 43 A GCM study of the atmospheric response to tropical SST
795 Anomalies. In: Nihoul JCJ (ed) Elsevier Oceanography Series. Elsevier, pp 749–764

796 Sutton RT, Hodson DLR (2005) Atlantic Ocean Forcing of North American and European Summer
797 Climate. Science 309:115–118. https://doi.org/10.1126/science.1109496

798 Sutton RT, Hodson DLR (2007) Climate Response to Basin-Scale Warming and Cooling of the
799 North Atlantic Ocean. J Climate 20:891–907. https://doi.org/10.1175/JCLI4038.1

Trenberth KE, Branstator GW (1992) Issues in Establishing Causes of the 1988 Drought over North America. J Climate 5:159–172. https://doi.org/10.1175/1520-0442(1992)005<0159:IIECOT>2.0.CO;2

Trenberth KE, Branstator GW, Arkin PA (1988) Origins of the 1988 North American Drought. Science 242:1640–1645. https://doi.org/10.1126/science.242.4886.1640

Trenberth KE, Guillemot CJ (1996) Physical Processes Involved in the 1988 Drought and 1993 Floods in North America. J Climate 9:1288–1298. https://doi.org/10.1175/1520-0442(1996)009<1288:PPIITD>2.0.CO;2

Vecchi GA, T. DELWORTH, R. GUDGEL, et al (2014) On the Seasonal Forecasting of Regional Tropical Cyclone Activity. J Climate 27:7994–8016. https://doi.org/10.1175/JCLI-D-14-00158.1

Walker GT (1924) Correlation in Seasonal Variations of Weather, IX. A Further Study of World Weather. Mem Indian Meteor Dep 24:275–332

Wallace J, Gutzler D (1981) Teleconnections in the geopotential height field during the Northern Hemisphere winter. Mon Weather Rev 109:784–812

Wang C, Lee S-K, Enfield DB (2008) Climate Response to Anomalously Large and Small Atlantic Warm Pools during the Summer. J Climate 21:2437–2450. https://doi.org/10.1175/2007JCLI2029.1

Zhang H (2020) Tropical Pacific intensifies June extreme rainfall over Southwestern United States/Northwestern Mexico. Clim Dyn. https://doi.org/10.1007/s00382-020-05291-6

822 Table 1. Simulations.

Experiments	Forcing	Length (yr)
FLOR	preindustrial-level atmospheric composition and radiation (the same for all experiments), flux adjustment	3500
AM2.5	driven by climatological annual cycle of SST and sea ice from last 1000 years of FLOR	1000
Globe_1-12	as AM2.5, but driven by monthly varying SSTs from 600 years of FLOR over entire globe and for all months	600
Tropic_1-12	as AM2.5, but driven by monthly varying SSTs from 600 years of FLOR over the tropics (35°N and 35°S) and for all months	600
Pacific_10-5	as AM2.5, but driven by monthly varying SSTs from 600 years of FLOR over the tropical Pacific (35°N and 35°S) and only from October to May	600
Atlantic_5-10	as AM2.5, but driven by monthly varying SSTs from 600 years of FLOR over the tropical Atlantic (35°N and 35°S) and only from May to October	600

823 Note that preindustrial radiative forcing is nearly in balance at top of the atmosphere and thus
824 more suitable for millennium-long steady state simulations than present-day conditions.
825

826 **Figures**

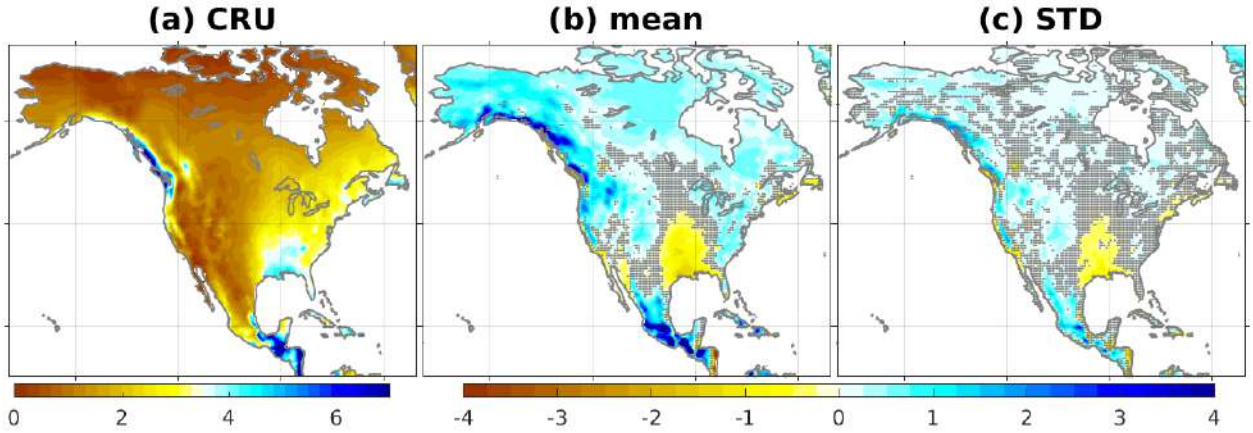

827
828 **Fig. 1** Precipitation (mm/day) biases in FLOR compared to observations. (a) 1981-2010 CRU
829 climatology; FLOR biases (FLOR – CRU) in (b) climatology and (c) standard deviation.
830 Stippling is a measure of insignificance, indicating at least one of CRU and GPCC is inside the
831 range of a synthetic 33-member FLOR ensemble, which is constructed by sampling the 1000-
832 year FLOR simulation with a 30-year (to mimic 1981-2010) non-overlapping period.
833

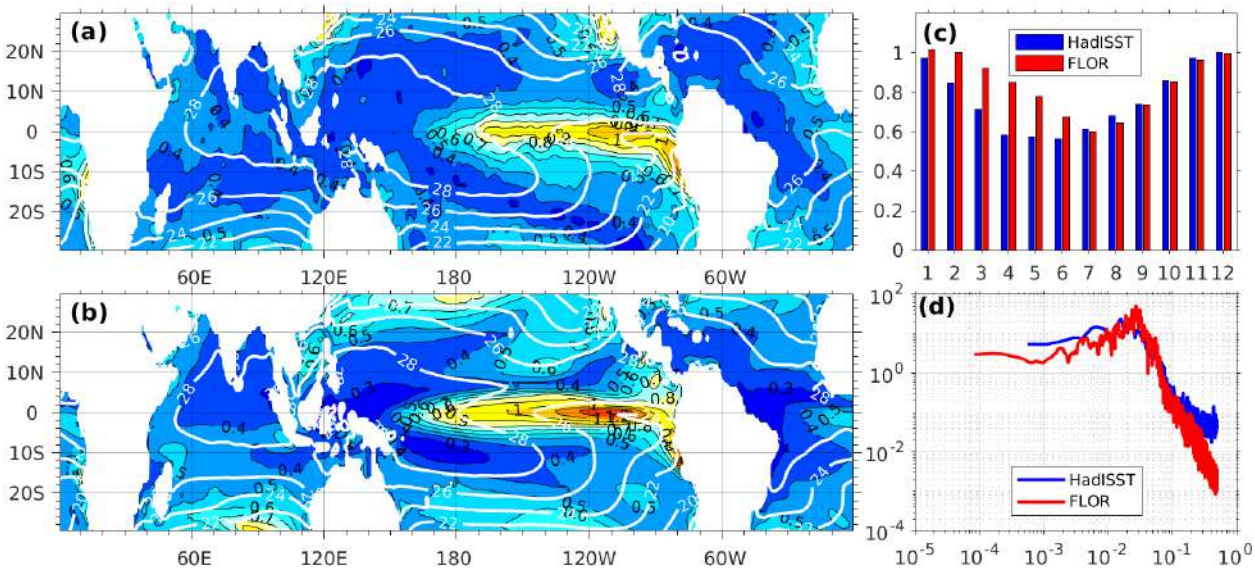

834

835 **Fig. 2** Tropical SST variability (°C) in FLOR versus HadISST 1870-2018. SST standard
836 deviation (shading) and climatology (white contours) in HadISST (a) and FLOR (b); monthly
837 standard deviation (c) and spectrum (d) of the Niño3.4 index (SST time series averaged over
838 170°W-120°W,5°N-5°S). The spectrum is normalized by the variance of the Niño3.4 index. X-
839 axis has a unit of calendar month in (c) and frequency of per month in (d), respectively.
840

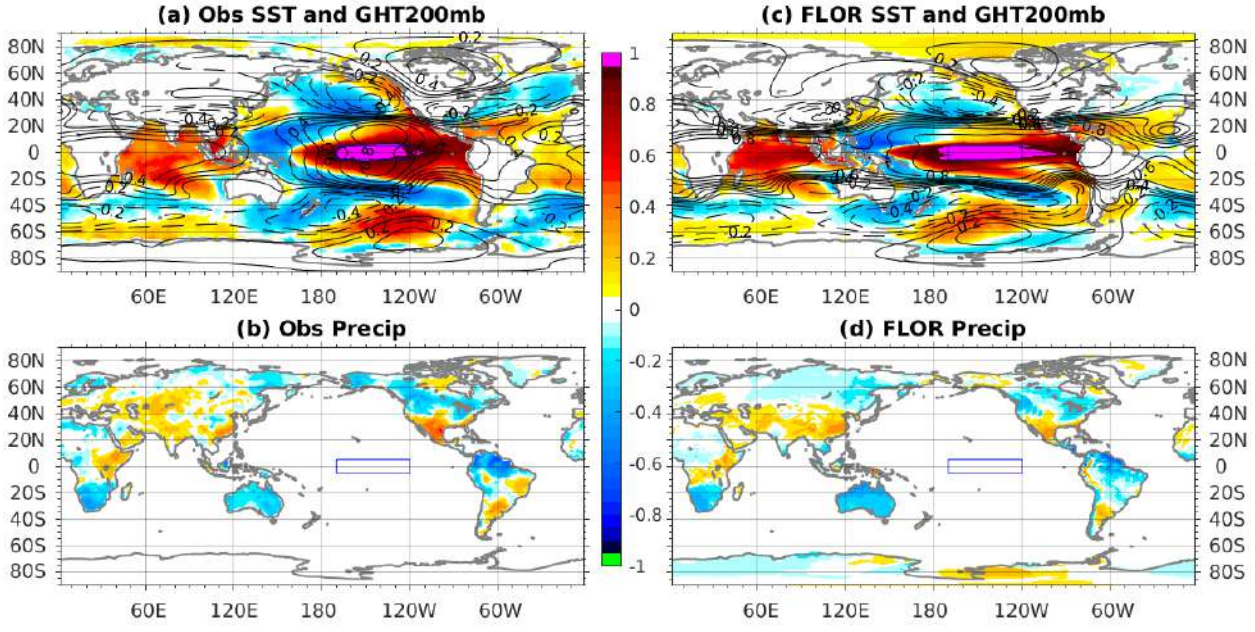

841

842 **Fig. 3** ENSO teleconnection in observations 1901-2012 (a, b) and FLOR (c, d). Teleconnection
843 is assessed during DJF as correlation coefficients between the Niño3.4 index and SST (shading),
844 200mb geopotential height (black contours) in (a, c), land precipitation in (b, d). Here 112 years
845 are used for observations, while 1000 years are used for FLOR. Random sampling of 112-year
846 segments from FLOR leads to small changes in correlation pattern and magnitude (not shown).
847

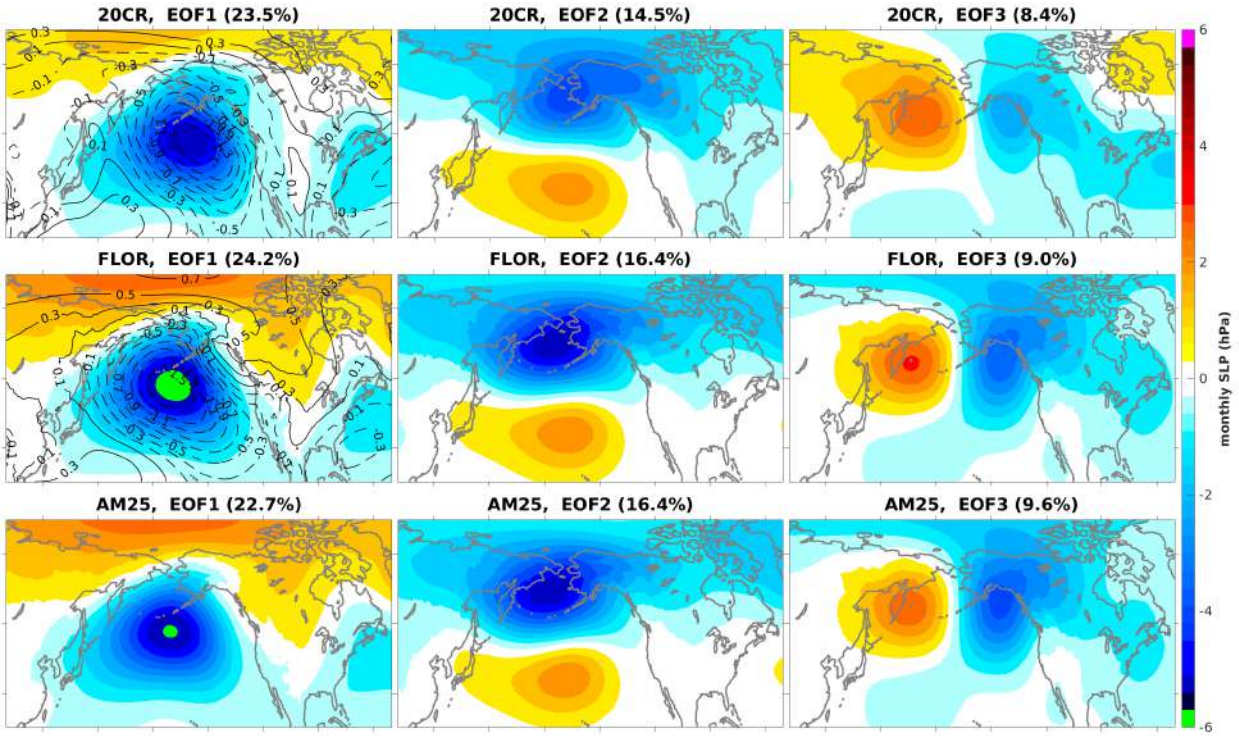

Fig. 4 Midlatitude variability of monthly SLP (hPa) in observations (top row), FLOR (middle row) and AM2.5 (bottom row). The leading three EOF modes are shown with their explained variance inside the parentheses above each panel. Contours (positive solid and negative dashed) in the EOF1 panels (left column, top two rows) are the regression coefficients (hPa/K) of monthly SLP anomaly against the Niño3.4 index, a measure of the ENSO teleconnection.

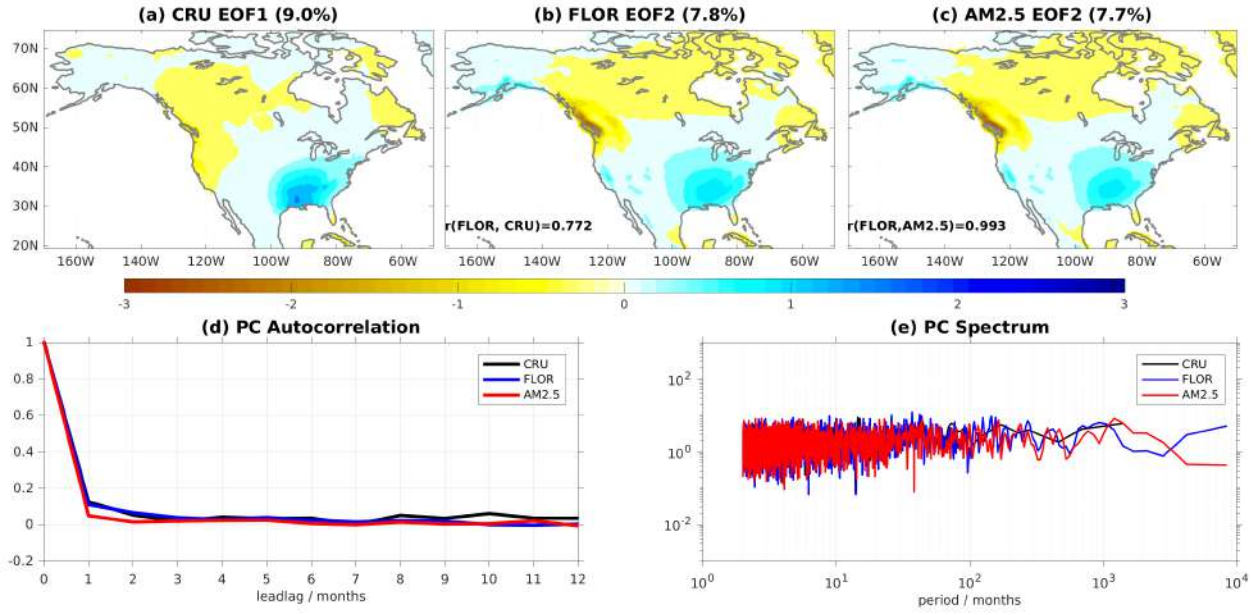

Fig. 5 Top row: (a) the first EOF mode in CRU observations and the second EOF mode in (b) FLOR and (c) AM2.5. The explained variance percentage is denoted above each panel. Pattern correlation is 0.772 between CRU and FLOR and 0.993 between FLOR and AM2.5. Bottom row: (d) the associated PC autocorrelation and (e) spectrum.

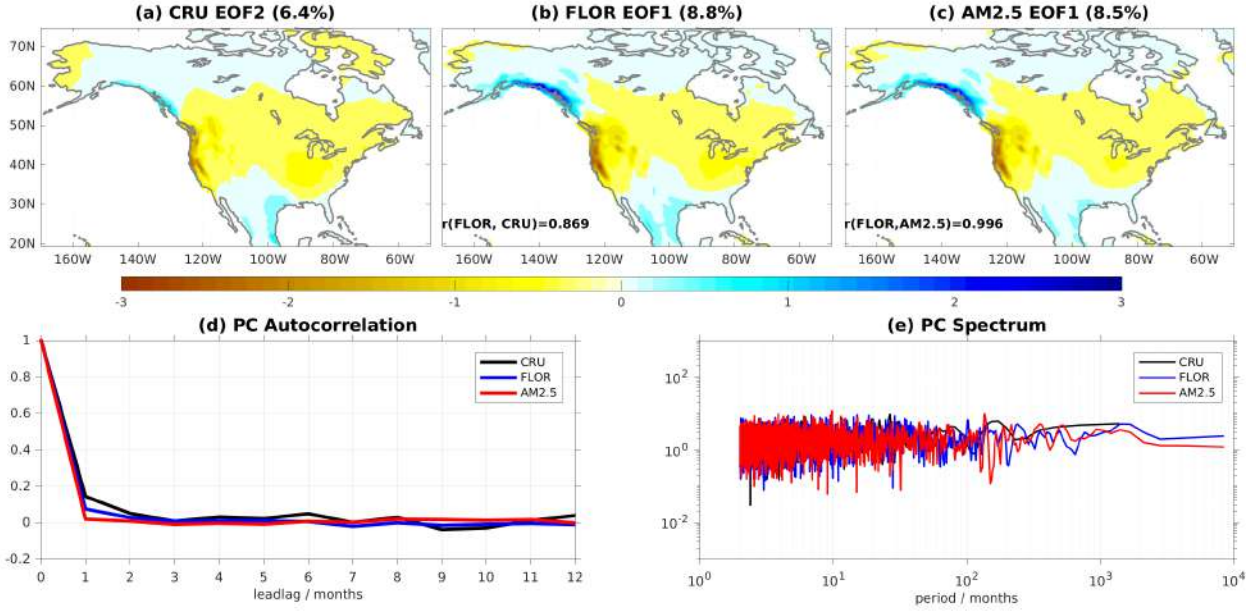

Fig. 6 The same as Fig. 5 but for the second EOF mode in observations and the first EOF mode in FLOR and AM2.5. Pattern correlation is 0.869 between CRU and FLOR and 0.996 between FLOR and AM2.5.

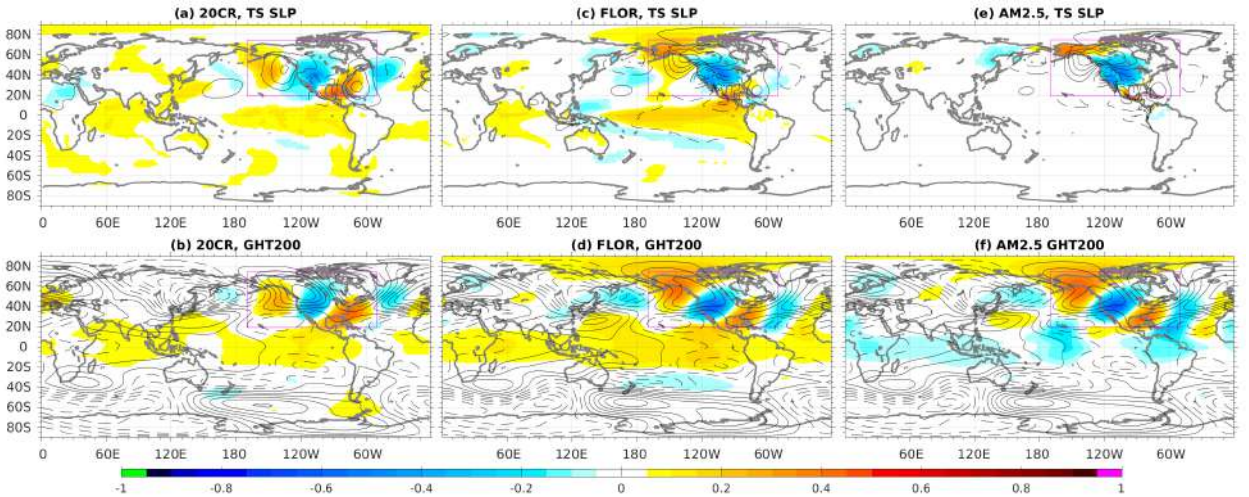

Fig. 7 Large-scale pattern of correlation coefficients between the PCs of the EOF modes in Fig. 5 (reflecting precipitation variability over the southeastern United States) and surface temperature (shading in top row), SLP (contours in top row) and 200mb geopotential height (shading in bottom row) in observations (left column, 20CR dataset), FLOR (middle column) and AM2.5 (right column). Contours in the bottom row are the departure of climatological GHT200 from its zonal mean, denoting climatological stationary eddies. Contour interval is 0.1 for SLP

correlation and 20m for GHT200, and solid (dashed) contours denote positive (negative) values (zeros omitted). The magenta box in each panel denotes the region where the EOF decomposition is conducted.

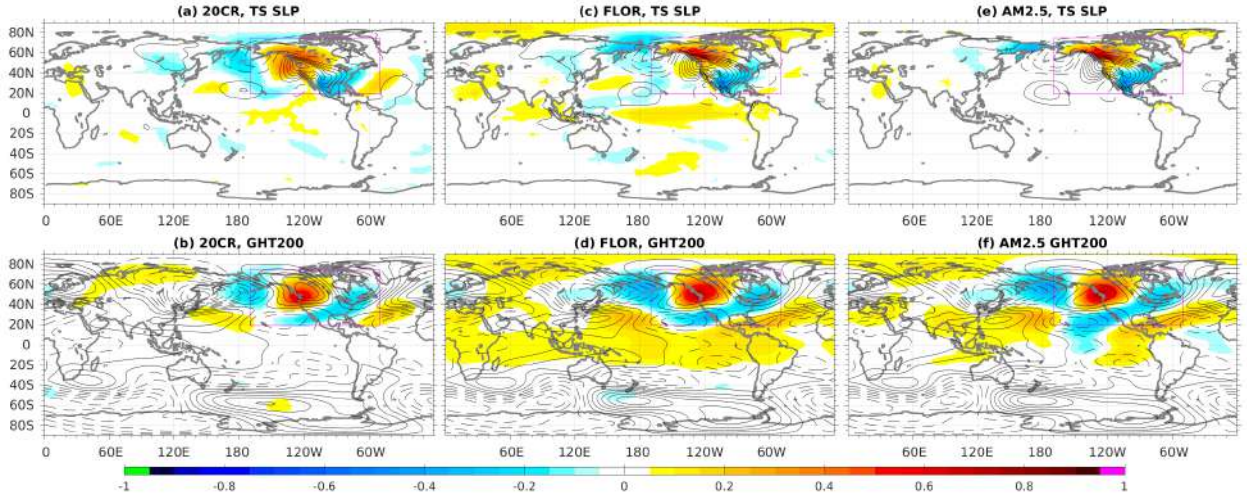

Fig. 8 The same as Fig. 7 but for the EOF modes shown in Fig. 6 (reflecting precipitation variability over the Pacific Northwest).

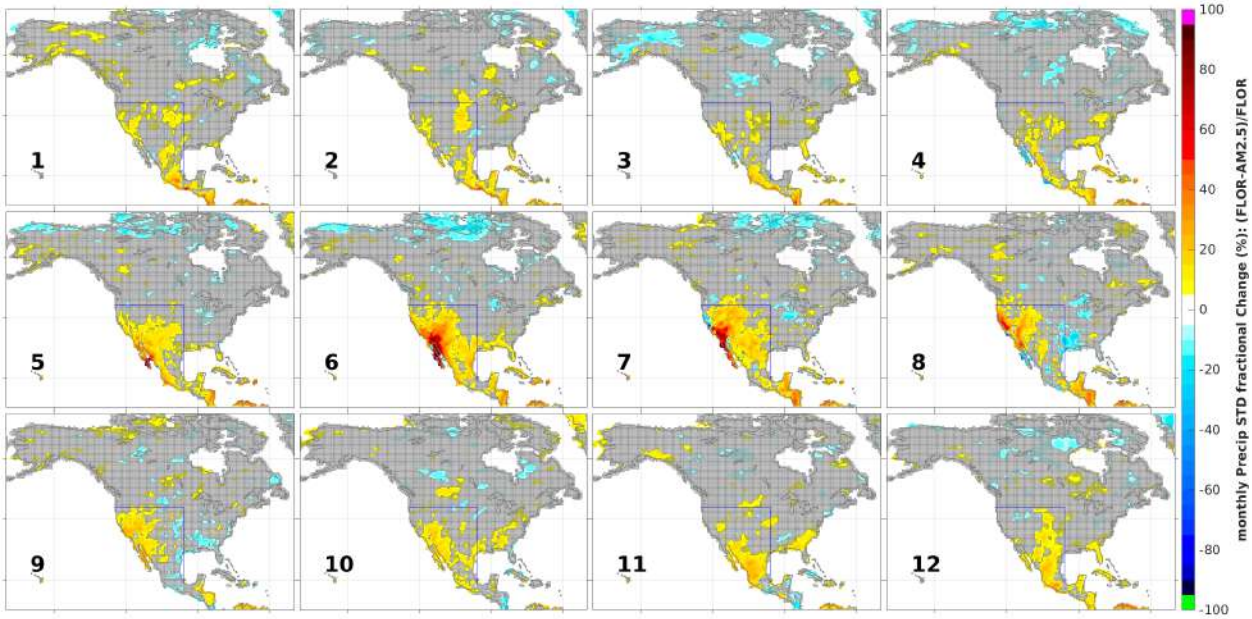

Fig. 9 Fractional change (%) in year-to-year standard deviation of monthly precipitation between FLOR and AM2.5 as a function of calendar month, defined as (FLOR-AM2.5)/FLOR*100%. Gray stippling indicates changes are not significant at the 1% level based on a two-sided Fisher test. The blue transposed 'L' outlines the SWNA region where the month-to-month variance of monthly precipitation (Fig. 12a) is significantly enhanced by the ocean in FLOR relative to AM2.5.

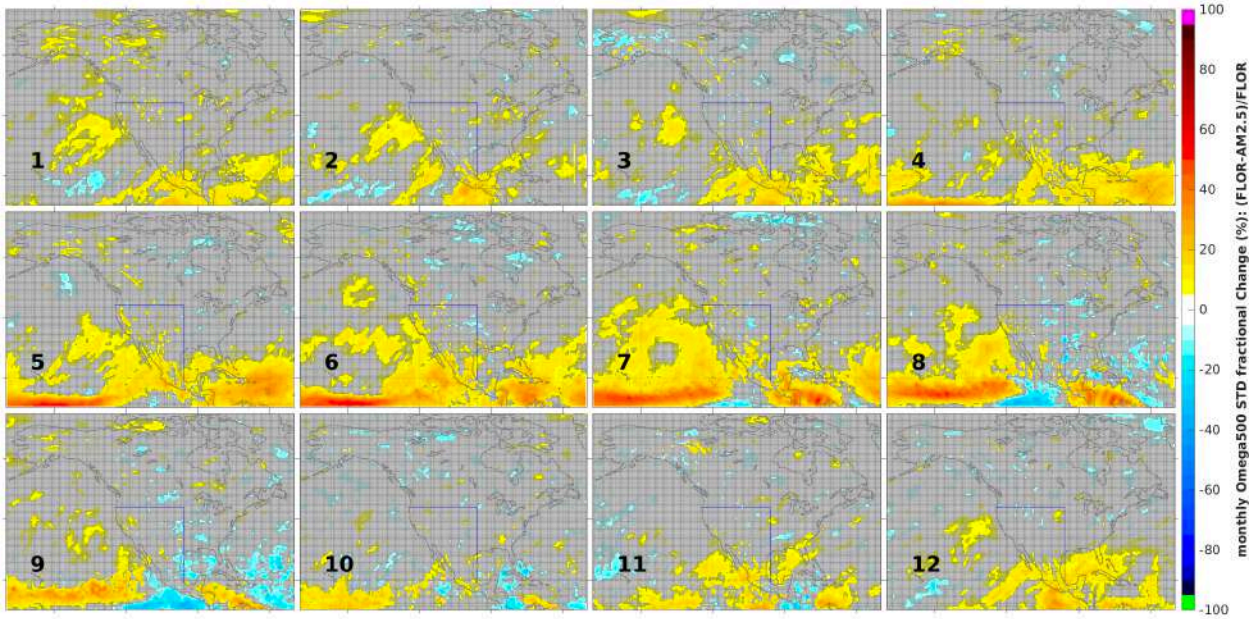

Fig. 10 The same as Fig. 9 but for 500mb omega.

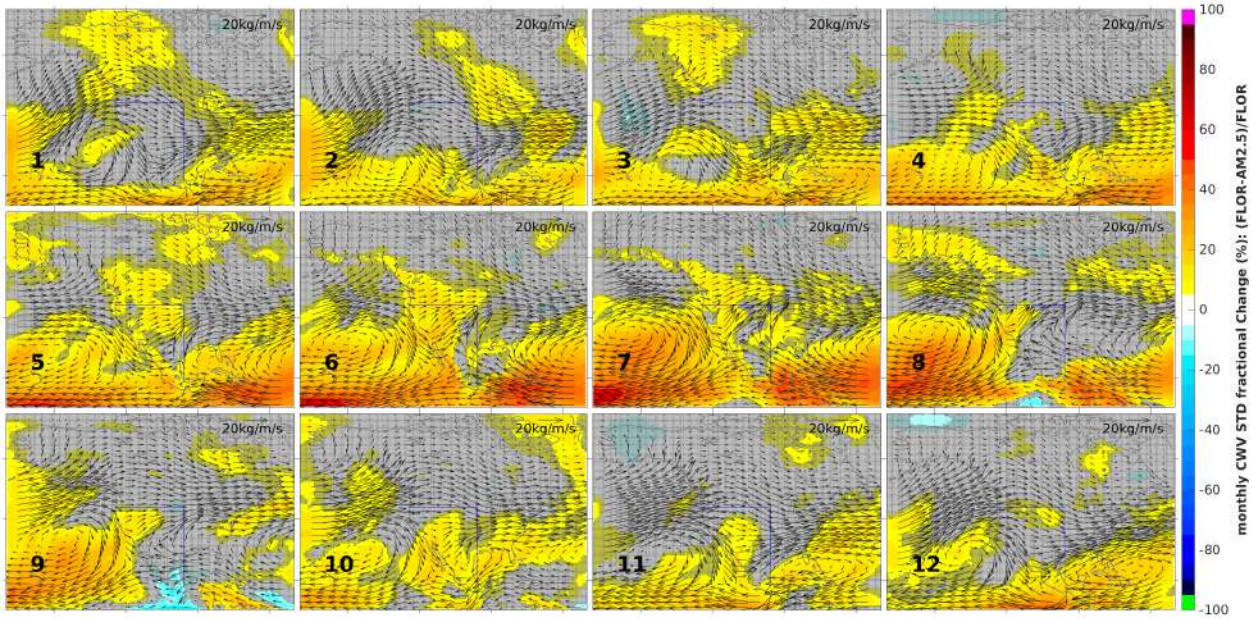

Fig. 11 The same as Fig. 9 but for CWV (atmosphere moisture content). Vectors denote the vertically integrated flux of standard deviation of specific humidity by mean circulation (kg/m/s). A scale vector of 20kg/m/s is shown in the upper right corner of each panel.

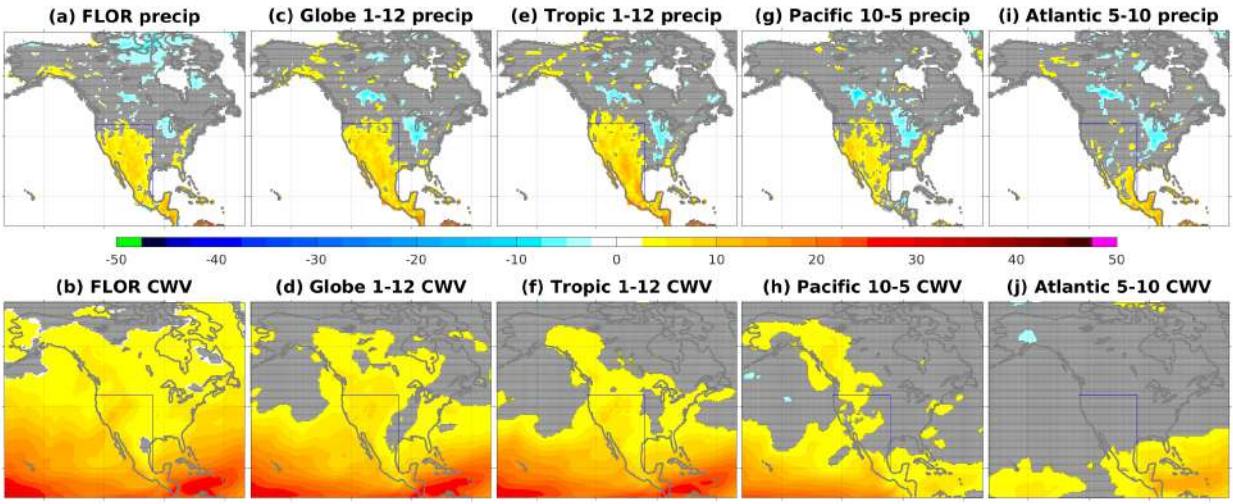

Fig. 12 Fractional change (%) in monthly precipitation (top row) and CWV (bottom row) month-to-month standard deviation in FLOR (a-b), Globe_1-12 (c-d), Tropic_1-12 (e-f), Pacific_10-5 (g-h) and Atlantic_5-10 (i-j) with respect to AM2.5. Gray stippling indicates changes are not significant at the 1% level based on a two-sided Fisher test. The blue 'L' outlines the SWNA region.

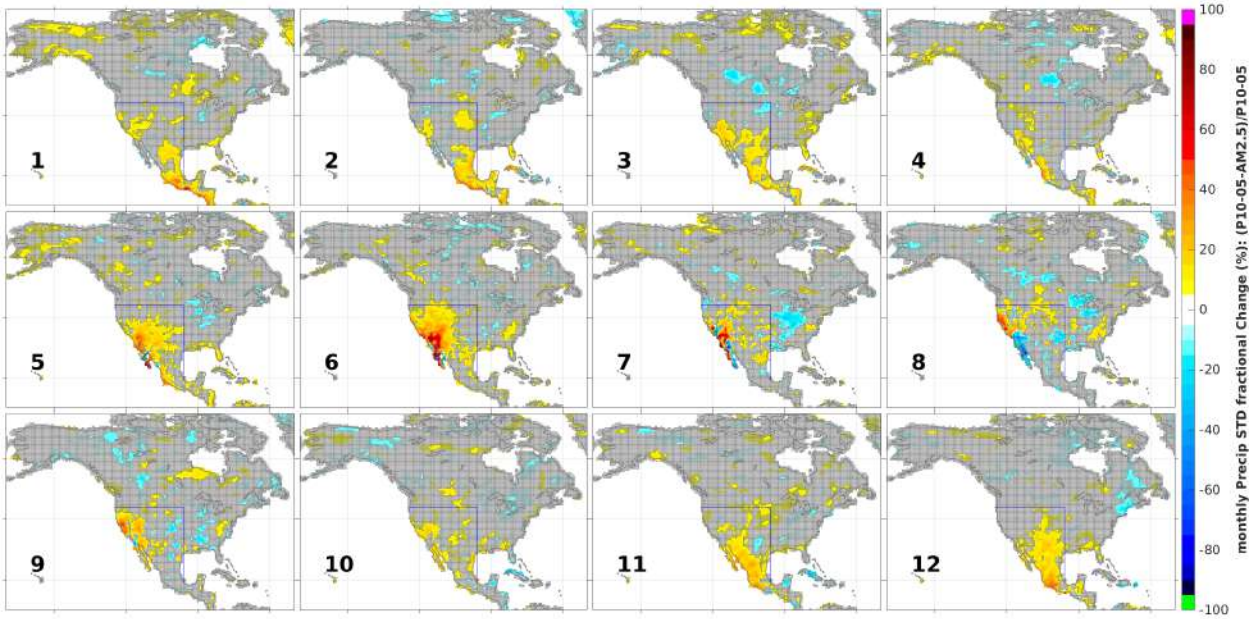

Fig. 13 The same as Fig. 9 but for Pacific_10-5.

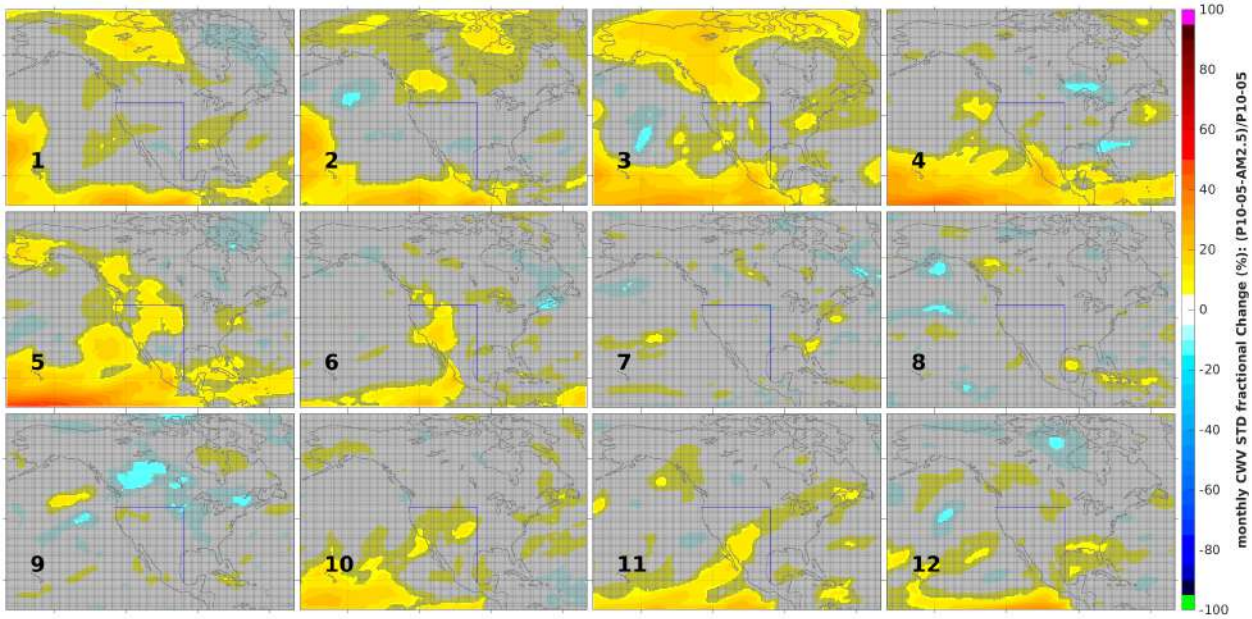

Fig. 14 The same as Fig. 13 but for CWV in Pacific_10-5.

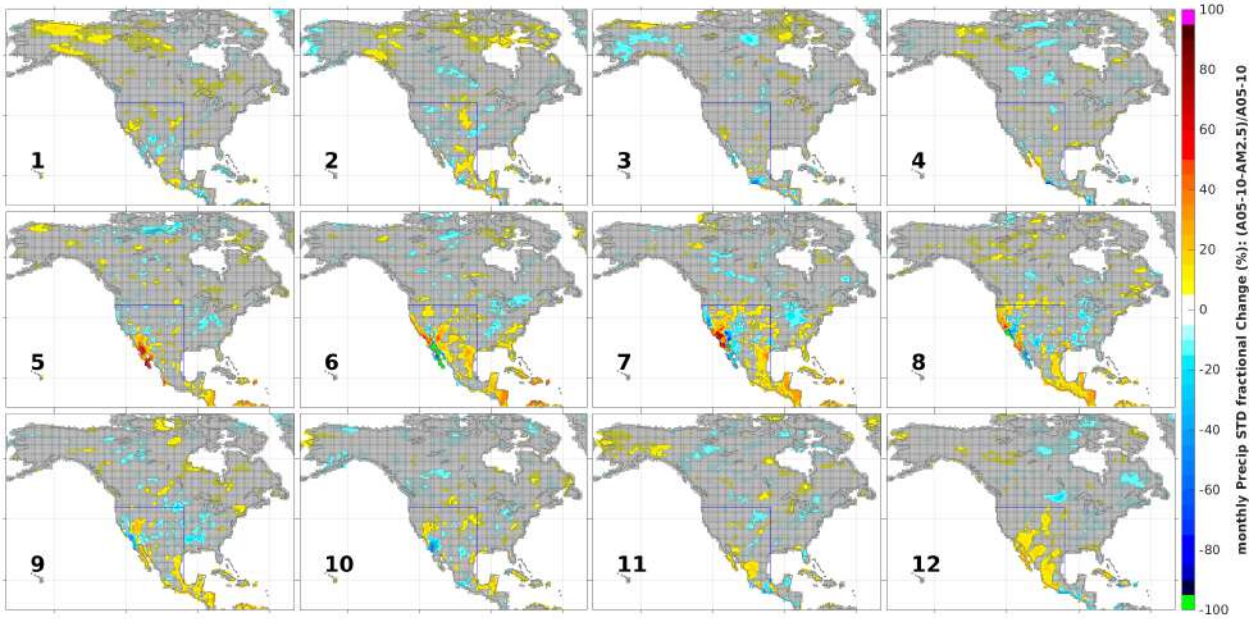

Fig. 15 The same as Fig. 13 but for Atlantic_5-10.

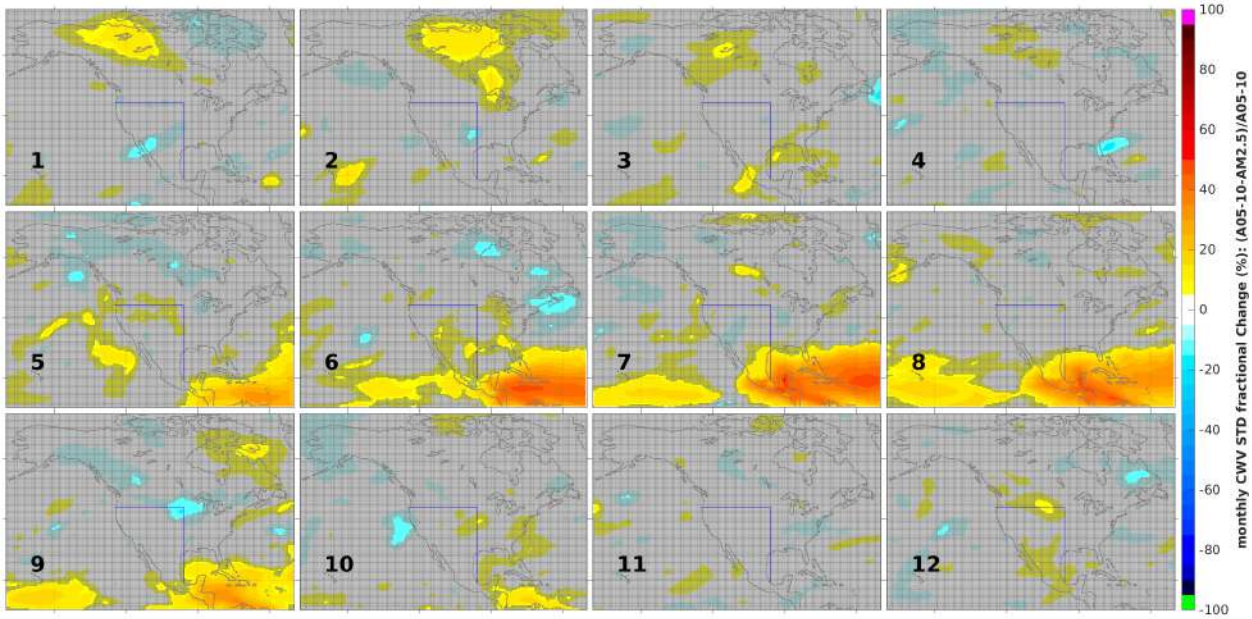

Fig. 16 The same as Fig. 15 but for CWV in Atlantic_5-10.

Appendix

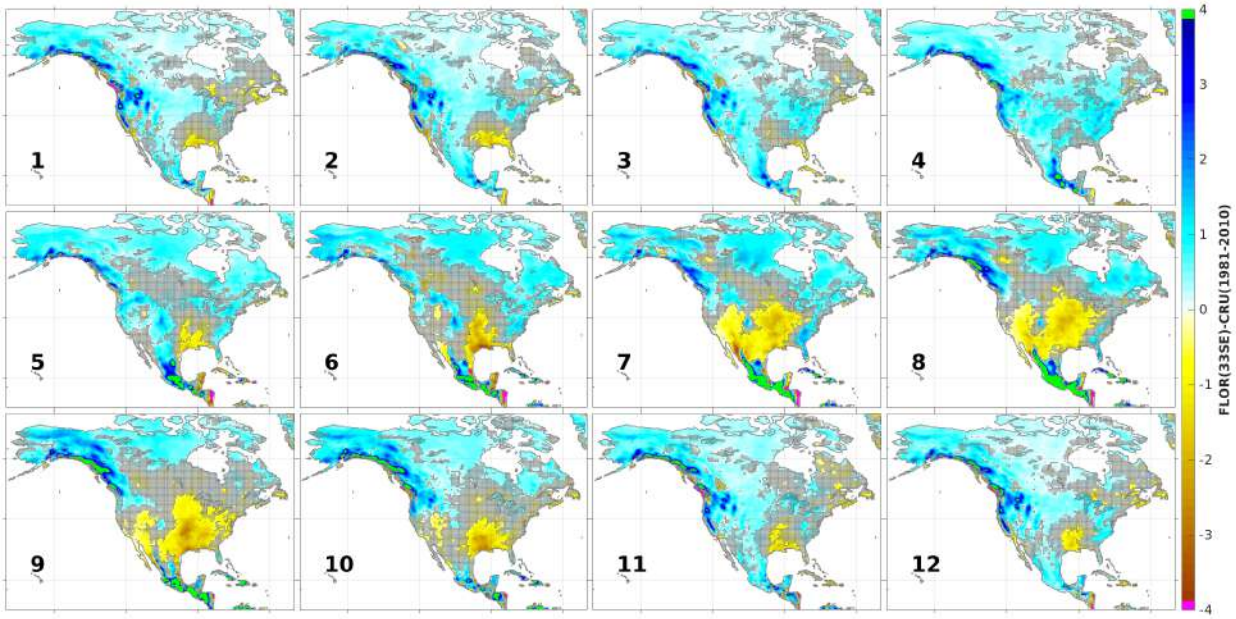

Fig. 17 Biases of monthly precipitation climatology (mm/day) in FLOR compared to the 1980-2010 CRU and GPCC observations. Shown here is FLOR – CRU. Stippling is measure of insignificance, indicating either CRU or GPCC climatology is inside the range of a synthetic 33-member FLOR ensemble, which is constructed by sampling the 1000-year FLOR simulation with a 30-year non-overlapping period.

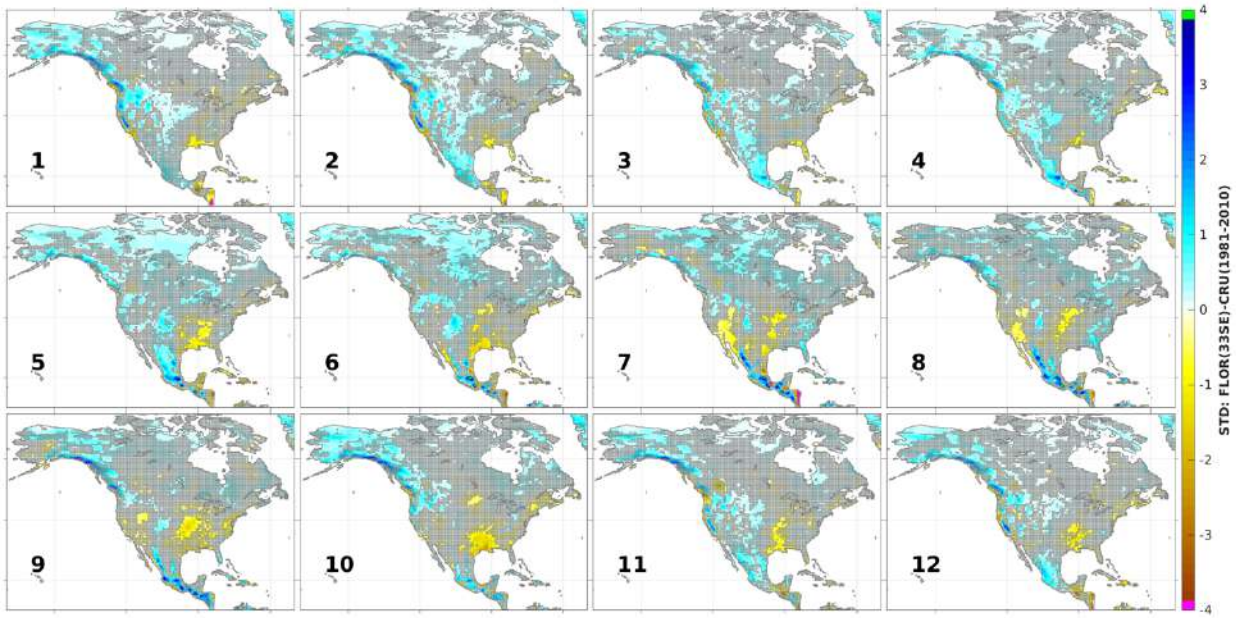

Fig. 18 Biases in year-to-year standard deviation of monthly precipitation (mm/day) over North America in FLOR compared to the 1980-2010 CRU and GPCC observations. Stippling is a measure of insignificance, indicating either CRU or GPCC standard deviation is inside the range

of a synthetic 33-member FLOR ensemble, which is constructed by sampling the 1000-year FLOR simulation with a 30-year non-overlapping period.

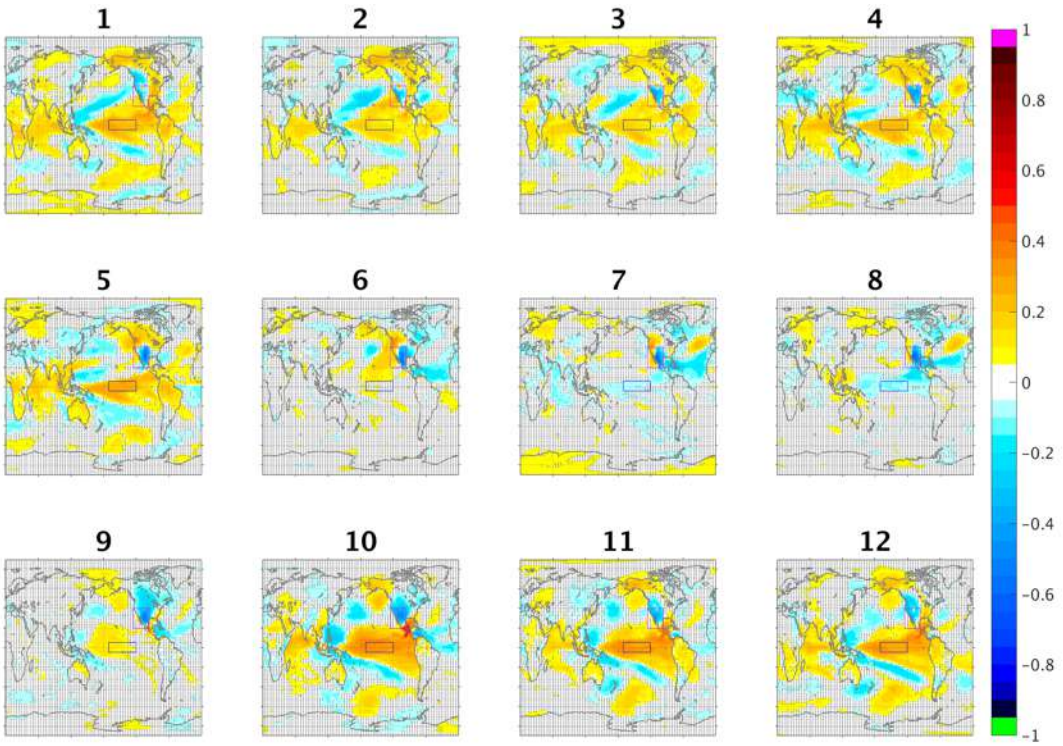

Fig. 19 Correlation of monthly surface temperature with monthly precipitation averaged over southwestern North America (19-40°N, 125-96°W, indicated by a red box in each panel) as a function of calendar months in FLOR. Gray stippling denotes that the correlation is not significant at 5% level (based on a two-sided student t test). Note that this figure has been published in Zhang (2020, Fig. 13).

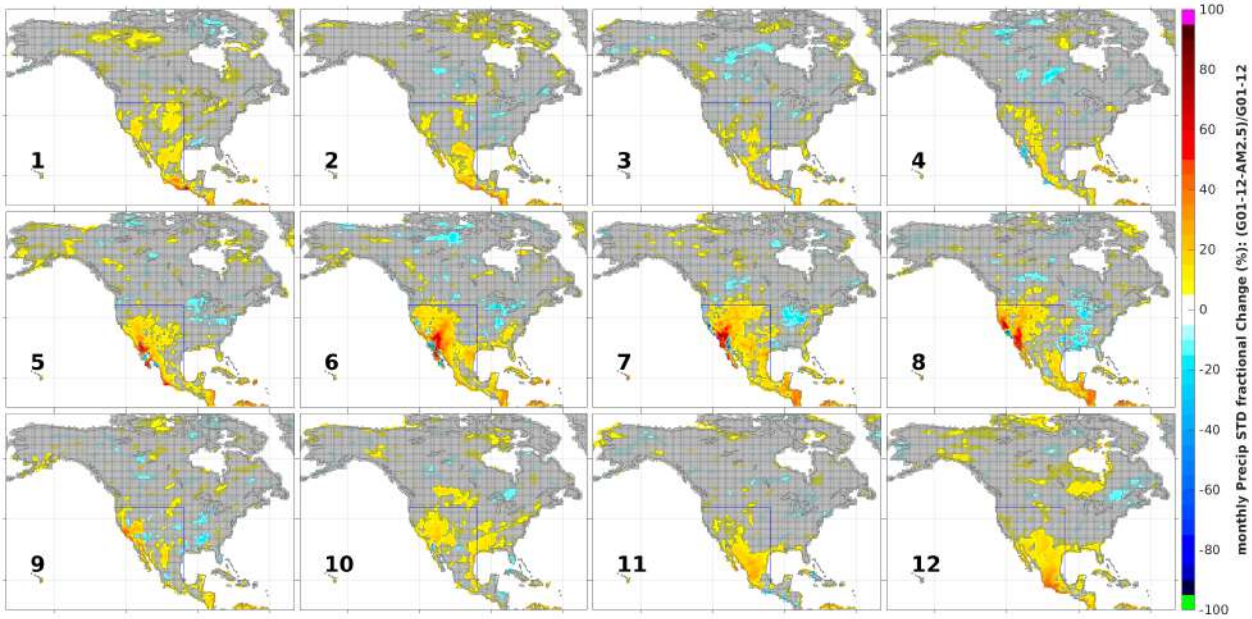

Fig. 20 Fractional change (%) in year-to-year standard deviation of monthly precipitation in Globe_1-12 relative to AM2.5, (Globe_1-12 - AM2.5)/Globe_1-12*100%, as a function of calendar month. Gray stippling indicates changes are not significant at the 1% level based on a two-sided Fisher test.

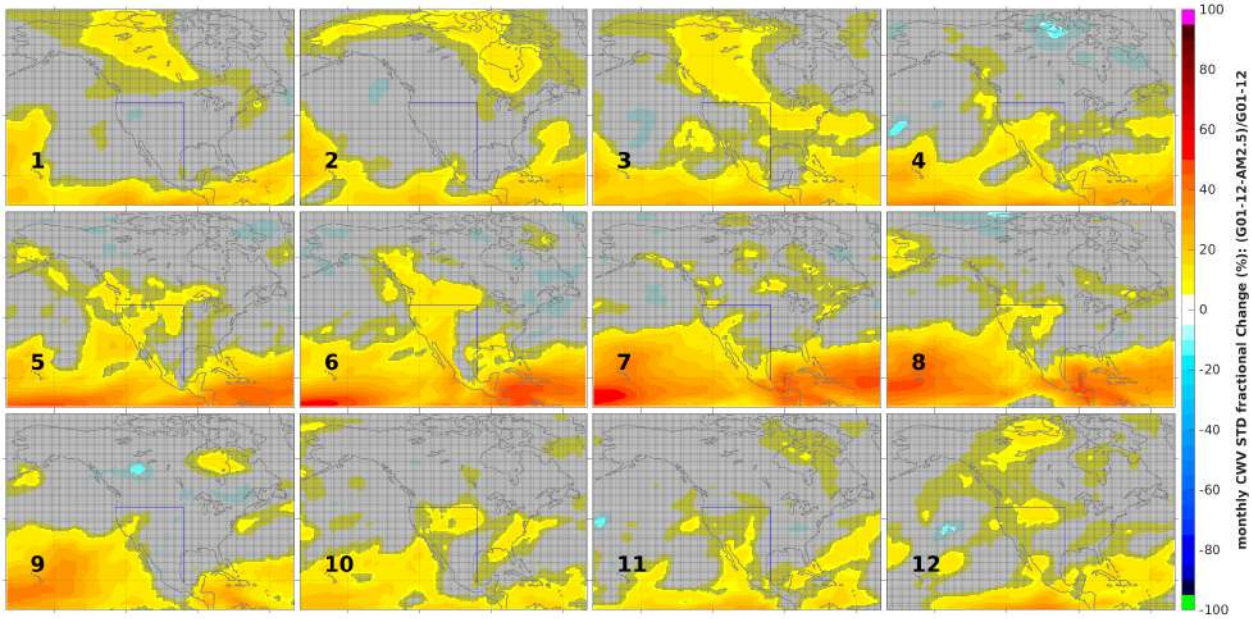

Fig. 21 The same as Fig. 20 but for CWV in Globe_1-12.

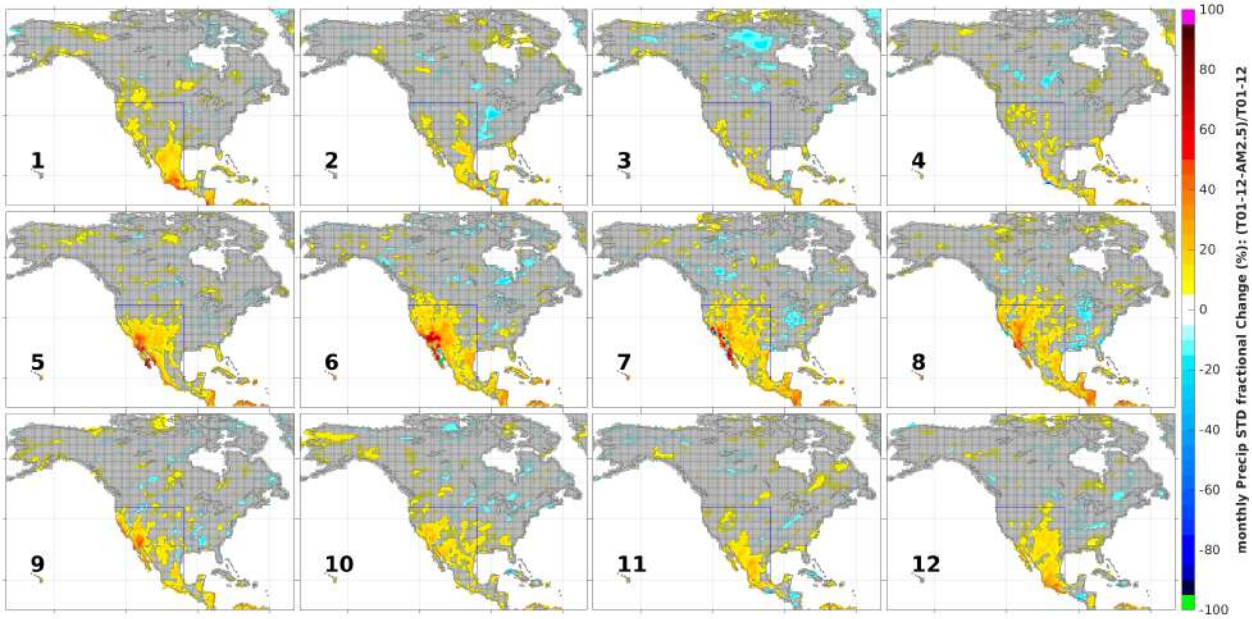

Fig. 22 The same as Fig. 20 but for Tropic_1-12.

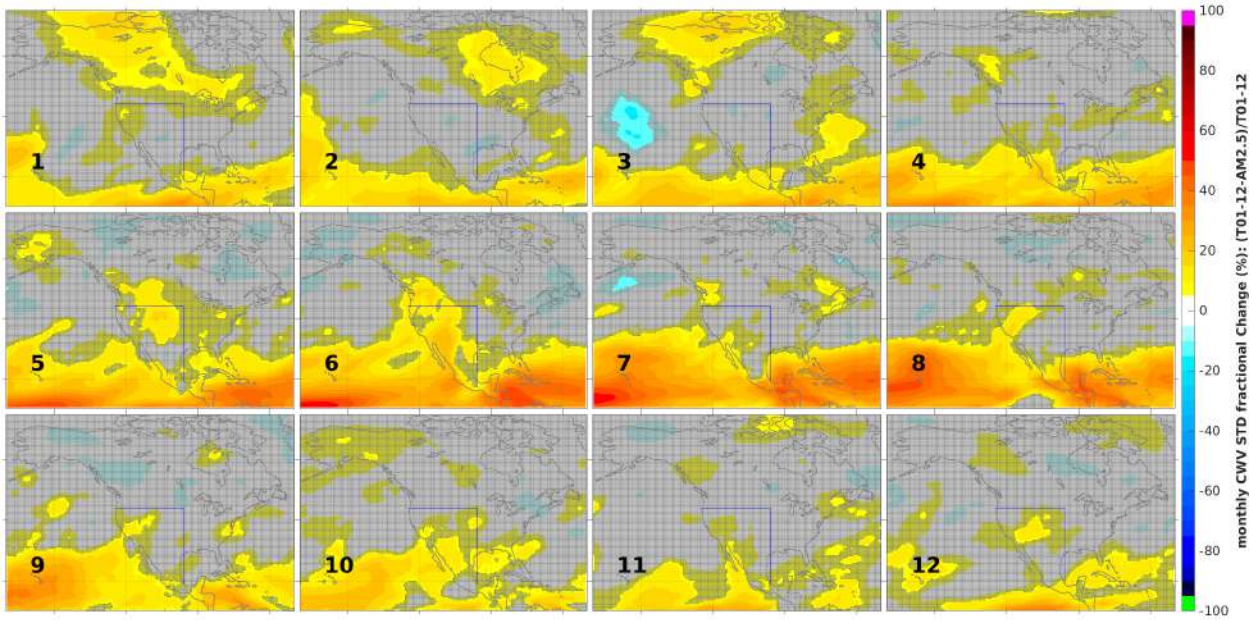

Fig. 23 The same as Fig. 22 but for CWV in Tropic_1-12.